Mitochondrial creatine sensitivity is lost in the D2. mdx model of Duchenne muscular dystrophy and rescued by the mitochondrial-enhancing compound Olesoxime

Catherine Bellissimo, Luca Delfinis, Meghan Hughes, Patrick Turnbull, Shivam Gandhi, Sara Dibenedetto, Fasih Rahman, Peyman Tadi, Christina Amaral, Ali Dehghani, et al.

RESEARCH ARTICLE

Mitochondrial creatine sensitivity is lost in the D2.*mdx* model of Duchenne muscular dystrophy and rescued by the mitochondrial-enhancing compound Olesoxime

Catherine A. Bellissimo,[1] Luca J. Delfinis,[1] Meghan C. Hughes,[1] Patrick C. Turnbull,[1] Shivam Gandhi,[1] Sara N. DiBenedetto,[1] Fasih A. Rahman,[2] Peyman Tadi,[1] Christina A. Amaral,[1] Ali Dehghani,[1] James N. Cobley,[3] Joe Quadrilatero,[2] Uwe Schlattner,[4] and Christopher G. R. Perry[1]

[1]*School of Kinesiology & Health Science, Muscle Health Research Centre, York University, Toronto, Ontario, Canada;* [2]*Faculty of Health, Department of Kinesiology and Health Sciences, University of Waterloo, Waterloo, Ontario, Canada;* [3]*Redox Biology Group, Centre for Health Sciences, University of the Highlands and Islands, Inverness, United Kingdom; and* [4]*Laboratory of Fundamental and Applied Bioenergetics, University Grenoble Alpes, Inserm U1055, Grenoble, France and Institut Universiatire de France Paris, France*

Abstract

Duchenne muscular dystrophy (DMD) is associated with distinct mitochondrial stress responses. Here, we aimed to determine whether the prospective mitochondrial-enhancing compound Olesoxime, prevents early-stage mitochondrial stress in limb and respiratory muscle from D2.*mdx* mice using a proof-of-concept short-term regimen spanning 10–28 days of age. As mitochondrial-cytoplasmic energy transfer occurs via ATP- or phosphocreatine-dependent phosphate shuttling, we assessed bioenergetics with or without creatine in vitro. We observed that disruptions in Complex I-supported respiration and mH$_2$O$_2$ emission in D2.*mdx* quadriceps and diaphragm were amplified by creatine demonstrating mitochondrial creatine insensitivity manifests ubiquitously and early in this model. Olesoxime selectively rescued or maintained creatine sensitivity in both muscles, independent of the abundance of respiration-related mitochondrial proteins or mitochondrial creatine kinase cysteine oxidation in quadriceps. Mitochondrial calcium retention capacity and glutathione were altered in a muscle-specific manner in D2.*mdx* but were generally unchanged by Olesoxime. Treatment reduced serum creatine kinase (muscle damage) and preserved cage hang-time, microCT-based volumes of lean compartments including whole body, hindlimb and bone, recovery of diaphragm force after fatigue, and cross-sectional area of diaphragm type IIX fiber, but reduced type I fibers in quadriceps. Grip strength, voluntary wheel-running and fibrosis were unaltered by Olesoxime. In summary, locomotor and respiratory muscle mitochondrial creatine sensitivities are lost during early stages in D2.*mdx* mice but are preserved by short-term treatment with Olesoxime in association with specific indices of muscle quality suggesting early myopathy in this model is at least partially attributed to mitochondrial stress.

muscle; neuromuscular disease; oxidative phosphorylation; permeability transition pore; reactive oxygen species

INTRODUCTION

Duchenne muscular dystrophy (DMD) is a debilitating and progressive muscle wasting disease resulting from a mutation in the gene encoding the protein dystrophin (1, 2). By connecting the cytoskeleton to the sarcolemma, dystrophin promotes membrane stability during muscle contraction and is a key component of the dystroglycan complex that cross-links the cytoskeleton to the extracellular matrix. The absence of dystrophin results in cell membrane instability and muscle fiber tearing during contraction (3). Constant cycles of fiber degeneration are associated with considerable inflammation as well as many intracellular stressors including elevated cytosolic calcium, cytoskeletal disorganization, and both redox and metabolic abnormalities. Each of these disruptions have been associated with mitochondrial stress responses (4), but the degree to which mitochondria contribute to muscle weakness in DMD remains to be determined.

The emergence of mitochondrial-enhancing therapeutics provides an opportunity to revisit the role of mitochondrial stress in a variety of diseases. However, in some cases, the potential clinical efficacy of the compounds somewhat outpaces the discovery of their mechanisms of action. For example, the cholesterol-based compound Olesoxime (cholest-4-en-3-one oxime, or TRO1966) promoted motor neuron survival, improved motor performance, and extended lifespan using in vitro and in vivo models of amyotrophic lateral sclerosis (ALS) (5). Although mitochondrial assessments were not performed in these models, separate experiments in a variety of brain-derived

cell lines found that Olesoxime accumulated in mitochondria (6) and interacted with the voltage-dependent anion channel (VDAC) (5). This protein was considered to be a putative component of the proapoptotic mitochondrial permeability transition pore (mPTP), and several effects attributed to mPTP inhibition were reported. These include reduced mitochondrial-linked apoptosis in cultured motor neurons (5), in a rat model of Huntington's (7) and camptothecin chemotherapy exposure (8), as well as other anti-mPTP effects in HeLa cells (6) and in cardiomyocytes exposed to doxorubicin chemotherapy (6). These lines of evidence suggest a potential to treat other conditions that present with dysregulated mPTP. However, the effect of Olesoxime on other mitochondrial bioenergetic functions in conditions causing mitochondrial stress remains unclear.

The degree to which Olesoxime may benefit muscle-weakness disorders remains uncertain. Clinical trials of Olesoxime in spinal muscle atrophy yielded mixed results (9–13). As some studies in mouse models of DMD reported increased mPTP (12–14) further investigation into the potential for Olesoxime to treat muscle weakness in *mdx* mice seems warranted, especially one with an expanded assessment of bioenergetic functions relevant to muscle weakness including oxidative phosphorylation and reactive oxygen species generation. We also assessed the ability of calcium stress to trigger mPTP given the excess cytosolic calcium in dystrophic fibers are thought to contribute to fiber degeneration, and Olesoxime's effects on calcium as a specific trigger of mPTP are less studied. As Olesoxime passed Phase I clinical trials for safety (15), any potential benefit of this drug in other disorders could be translated to clinical applications more rapidly.

In this study, we employed a short-term treatment protocol as a proof-of-principle design that targets the early stages of myopathy in the D2.*mdx* mouse model of DMD given we have previously characterized several relationships between muscle dysfunction and mitochondrial stress, including mPTP, at 4 wk of age in this model (14, 17, 18). Here, we report a novel effect by which Olesoxime protects mitochondrial bioenergetics by preserving the mitochondrial function of creatine. This effect was found in both locomotor and respiratory muscles, suggesting a ubiquitous mechanism. This improved mitochondrial creatine sensitivity was generally linked to preserving oxidative phosphorylation and attenuating increased mitochondrial hydrogen peroxide emission (mH$_2$O$_2$), but surprisingly not calcium-induced mPTP. This short-term treatment protocol at the early stages of the disease led to a robust reduction in the muscle damage marker serum creatine kinase as well as modest benefits to various indices of muscle quality. The findings indicate attenuated mitochondrial creatine functions may be one component of the stressors influencing early stages of myopathy during dystrophin deficiency which warrants longer term investigations.

MATERIALS AND METHODS

Animal Care

Male D2.*mdx* mice were bred from an in-house colony established at York University (Toronto, Ontario). Mice were housed with littermates until euthanasia (28 days) and then were separated for functional testing commencing 48 h before euthanasia. Three-week-old DBA/2J WT mice were ordered directly from Jackson Laboratories (Bar Harbor) due to low breeding performance experienced in-house as reported previously (19) and allowed to acclimatize for 7 days before euthanasia. Mice were maintained on a 12:12-h light-dark cycle while being provided access to standard chow and water ad libitum. All experiments and procedures were approved by the Animal Care Committee at York University (AUP Approval Number 2016-18) in accordance with the Canadian Council on Animal Care.

Olesoxime Treatment

D2.*mdx* mice were treated with Olesoxime (30 mg/kg body wt/day) dissolved in corn oil (5, 20, 21) or corn oil alone via oral gavage adapted for young pups (22). Treatment lasted from 10 days of age to 28 days (up to 30 days of age).

Body Composition and Functional Assays

In vivo computed tomography was assessed as previously described (14) with a threshold for fat-free mass set to 39–50 and normalized to body weight in grams. Voluntary wheel running, cage hang-time, and forelimb grip strength were assessed as described previously (14).

Minute Voluntary Movement Tracker

Voluntary ambulation was monitored according to the protocol established by Gibbs et al. (23). Animals were placed in an open-field container and movement was recorded for 6 min and analyzed using Kinovea software (kinovea.org). The cumulative distance moved in centimeters over the 6-min period was recorded.

Serum Creatine Kinase

Serum creatine kinase activity (U/L) was assessed spectrofluorometrically (QuantaMaster 80, HORIBA; emission 450 nm) using the Pointe Scientific Serum Creatine Kinase Kit (Pointe Scientific, Canton, MI) and calculated from the rate of NADPH production applied to a standard curve performed under the same conditions and volume dilution as samples.

In Vitro Diaphragm Force

Assessment of in vitro diaphragm force has been partially adapted from (24, 25). Briefly, the entire diaphragm was excised and placed in ice-cold Ringer solution containing (in mM) 121 NaCl, 5 KCl, 1.8 CaCl$_2$, 0.5 MgCl$_2$, 0.4 NaH$_2$PO$_4$, 24 NaHCO$_3$, 5.5 glucose, and 0.1 EDTA; pH 7.3. A diaphragm strip, no more than 3–4 mm in width, from the lateral costal hemidiaphragm was cut with adjacent sections of the rib and part of the central tendon as demonstrated in (26). Silk suture was attached to the central tendons and the ribs and secured in a bath with oxygenated Ringer's solution (95% O$_2$/5% CO$_2$) maintained at 25°C with ribs secured to the force transducer with an s hook and central tendon to the lever arm. The diaphragm was positioned between two platinum electrodes driven by a biphasic stimulator (Model 305 C; Aurora Scientific, Inc., Aurora, ON, Canada) and allowed to acclimatize for 30 min. The optimal resting length (L$_0$) was found using single twitches until the maximal force was attained. A force-frequency curve was performed (1, 10, 20, 40, 60, 80, 100, 120, and 140 Hz) with 1 min of rest between

contractions with a final 5-min rest period provided before a fatiguing protocol was performed (70 Hz for 350 ms every 2 s for 5 min). Recovery from fatigue was assessed at 5-, 10-, and 15-min post fatigue at the frequency that elicited maximum force in the force-frequency protocol. Force production was analyzed using Dynamic Muscle Control Data Acquisition software (Aurora Scientific, Inc) and normalized to cross-sectional area (CSA) of the muscle strip ($m/l \times d$) where m is the mass of the strip devoid of the central tendon and ribs, l is the length (from the point of insert on the ribs to the myotendinous junction of the central tendon), and d is the mammalian skeletal muscle density (1.06 g/mm^3) (27).

Preparation of Permeabilized Muscle Fiber Bundles

This technique was adapted from previous methods as described elsewhere (14, 28). Quadriceps and diaphragm muscles were excised carefully from mice while under heavy sedation using isoflurane. A piece of the nonstimulated quadriceps or diaphragm was removed and placed immediately into ice-cold BIOPS containing (in mM) 50 MES Hydrate, 7.23 K$_2$EGTA, 2.77 CaK$_2$EGTA, 20 imidazole, 0.5 dithiothreitol, 20 taurine, 5.77 Na$_2$ ATP, 15 Na$_2$ PCr, and 6.56 MgCl$_2$·6 H$_2$O (pH 7.1). Both muscles were trimmed of connective tissue and fat and separated along the longitudinal axis into small bundles weighing ∼1.0–2.5 mg wet weight for respiration and mH$_2$O$_2$ and 0.5–1.4 mg wet weight for calcium retention capacity. Bundles were permeabilized with 40 μg/μL saponin (Sigma Aldrich; St. Louis, MI) in BIOPS on a platform rotor for 30 min at 4°C. The permeabilized bundles were then transferred to wash buffers to remove saponin as follows: MiRO5 for mitochondrial respiration, Buffer Z for mitochondrial H$_2$O$_2$ emission (mH$_2$O$_2$), and Buffer Y for calcium retention capacity. The composition of each buffer has been described previously (14). Fibers prepared for Complex I-supported mitochondrial H$_2$O$_2$ emission (mH$_2$O$_2$) were permeabilized in the presence of 35 μM 2,4-dinitrochlorobenzene (CDNB) to deplete glutathione and allow for detectable rates of mH$_2$O$_2$ (29). All bioenergetic assays were performed within 4 h of washing to maintain fiber viability.

Mitochondrial Respiration

Mitochondrial respiration was performed as described in (14, 28). High-resolution oxygen consumption was performed in 2 mL of MiRO5 supplemented with (creatine-dependent) or without (creatine-independent) 20 mM creatine to saturate mitochondrial creatine kinase activity (28, 30) to permit assessments of mitochondrial creatine sensitivity. O$_2$ consumption was measured using the Oroboros Oxygraph-2K (Oroboros Instruments, Corp., Innsbruck, Austria) while stirring at 37°C in the presence of 5 μM blebbistatin to prevent spontaneous muscle fiber contraction in response to ADP (28). Each chamber was oxygenated with 100% pure O$_2$ to an initial concentration of ∼350 μM and experiments were completed before chamber [O$_2$] reached 150 μM (31, 32). Before permeabilization, fiber bundles were gently and quickly blotted, and weighed in ∼1.5 mL of tared cold BIOPS (ATP-containing relaxing media) to ensure fibers remained relaxed. Respiration was normalized to bundle wet weight. Complex I-supported respiration was stimulated using 5 mM pyruvate and 2 mM malate (NADH) followed by titration of ADP concentrations

from physiological ranges (25, 100) to supraphysiological (500) and saturating to stimulate maximal coupled respiration (5,000 μM). An addition of 10 μM cytochrome c was added to test mitochondrial outer membrane integrity. Experiments with low ADP-stimulated respiration (bundles that did not respire in response to ADP stimulus) or high cytochrome c responses (>15% increase in respiration) were removed (17 out of 192 bundles). Lastly, 20 mM succinate (FADH$_2$) was added to support Complex II respiration.

Mitochondrial H$_2$O$_2$ Emission

Mitochondrial H$_2$O$_2$ (mH$_2$O$_2$) emission was performed as described (14). mH$_2$O$_2$ was determined spectrofluorometrically (QuantaMaster 40, HORIBA Scientific, Irvine, CA) utilizing Buffer Z containing 10 μM Amplex Ultra Red (Life Technologies; Carlsbad, CA), 1 U/mL horseradish peroxidase, 1 mM EGTA, 40 U/mL Cu/Zn SOD1, 5 μM blebbistatin, and 20 mM Cr. Complex I-supported mH$_2$O$_2$ was initiated through the addition of 10 mM pyruvate and 2 mM malate (NADH; forward electron flow) and separately with 10 mM succinate (FADH$_2$; reverse electron flow from Complex II to I). The ability of ADP to suppress mH$_2$O$_2$ was assessed with a titration of physiological concentrations (25, 100) and saturating for oxidant generation (500 μM). All protocols were repeated without creatine in the assay buffer to permit comparisons with the creatine condition, thereby allowing assessments of mitochondrial creatine sensitivity. Bundles were lyophilized in a freeze-dryer (Labconco, Kansas City, MO) for >4 h and weighed on a microbalance (Sartorius Cubis Microbalance, Gottingen, Germany).

The rate of mH$_2$O$_2$ emission was calculated and converted to [mH$_2$O$_2$] using a standard curve under the same assay conditions and then normalized to fiber bundle dry weight.

Mitochondrial Calcium Retention Capacity

Mitochondrial calcium retention capacity was performed as previously described but with modifications (14, 33). This assay was measured spectrofluorometrically (QuantaMaster 80, HORIBA Scientific) in a cuvette with 300 μL assay buffer containing 1 μM Calcium Green-5N (Invitrogen), 2 μM thapsigargin, 5 μM blebbistatin, and 40 μM EGTA while maintained at 37°C with continuous stirring. 5 mM glutamate, 2 mM malate, 5 mM ADP, and 20 mM creatine were added to the assay buffer and minimum fluorescence was recorded. 4 nmol pulses of CaCl$_2$ were added until the mitochondrial permeability transition pore (mPTP) opening was observed as an increase in fluorescence corresponding to net mitochondrial calcium release, at which point saturating pulses of CaCl$_2$ were used to establish maximum fluorescence. Changes in free Ca^{2+} during mitochondrial Ca^{2+} uptake were then calculated using the known K_d for Calcium Green-5N and equations established for calculating free ion concentration (34). Calcium retention was then normalized to fiber bundle dry weight.

Histochemical and Immunofluorescent Staining

Excised quadriceps and diaphragm were mounted for histology and immunofluorescence in Tissue Plus Optimal Cutting Temperature compound (OCT; Fisher Healthcare), frozen in isopentane chilled in liquid nitrogen and stored at −80°C. The sample collected were cut into 10-μm thick serial cross sections with a cryostat (Thermo Fisher Scientific;

Kalamazoo, MI) maintained at $-20°C$ on Fisherbrand Superfrost Plus slides (Thermo Fisher Scientific). Hematoxylin and eosin (H&E) and picrosirius red (PSR) staining were used to assess muscle health and fibrosis as previously described (14). Centralized nuclei, a marker of regenerating fibers, was analyzed by selecting five evenly spaced images throughout the muscle and averaging the result. Areas of necrosis (fibers with fragmented sarcoplasm and immune cell infiltration) were expressed as a percentage of the entire muscle section. PSR staining was used to assess fibrotic regions and was expressed as a percentage of whole muscle section. Images were taken using EVOS M7000 imager (Thermo Fisher Scientific) using $×20$ magnification and analyzed using ImageJ (http://imagej. nih.gov/ij/). Immunofluorescent analysis of myosin heavy chain expression was previously described (35). Images were taken with EVOS M7000 equipped with standard red, green, and blue filter cubes. Fibers that were not positively stained were considered IIX fibers. These images were then analyzed with ImageJ for fiber type distribution and cross-sectional area (CSA).

Caspase Activity

The enzymatic activities of caspase 3, 8, and 9 were measured spectrofluorometrically using substrates Ac-DVED-AMC, AC-IETD-AMC, and Ac-LEHD-AMC (Enzo Life Sciences, Farmingdale, NY) respectively, as described elsewhere (36, 37). Samples were homogenized in ice-cold lysis buffer without protease inhibitors and pipetted into a 96-well plate where they were incubated with an appropriate substrate. Fluorescence was read for 1 h and maximal activity was recorded and normalized to the total protein content.

Glutathione

Reduced glutathione (GSH) and oxidized glutathione (GSSG) were assessed by UV-HPLC and fluorescent HPLC respectively using the Shimadzu Nexera X2 UHPLC system (Mandel Scientific Company Inc. Guelph, Canada). Quadriceps and diaphragm muscles were prepared according to Ref. 38 in tris buffer [50 mmol/L Tris (hydroxymethyl) amino methane buffer containing 20 mmol/L Boric acid, 2 mmol/L L-serine, 20 μmol/L Acivicin, and 5 mmol/L N-ethylmaleimide (NEM)] and acidified using TCA and PCA for GSH and GSSG, respectively. Separation was achieved using a Zorbax C18 column (Agilent Technologies, Mississauga, ON, Canada). GSH was measured under isocratic conditions by monitoring NEM-GSH using a 0.25% glacial acetic acid mobile phase with 6% acetonitrile at 1.05 mL/min flow rate detected at 265 nm. GSSG was measured using GS-o-pthalymide (0.1%) conjugate excited at 350 nm and detected at 420 nm emission using HPLC/UHPLC fluorescence detector (Mandel Scientific). GSSG samples were diluted in 0.5 M NaOH and run using 25 mM Na_2HPO_4 in HPLC-grade H_2O with 15% methanol mobile phase at a 0.5 mL/min flow rate. Distinct standard curves were applied to both GSH and GSSG and all samples were normalized to protein content measured using bicinchoninic acid protocols (Life Technologies, Carlsbad, CA).

Western Blotting

Western blotting was performed to determine expression levels of VDAC, adenine nucleotide translocase (ANT),

electron transport chain proteins (OXPHOS), and mitochondrial creatine kinase (mtCK) using standard SDS-PAGE procedures. Frozen sections of quadriceps and diaphragm from each muscle ($\sim$10–30 mg in size) were homogenized using a plastic microcentrifuge tube with tapered Teflon pestle in ice-cold buffer containing (in mM) 40 HEPES, 120 NaCl, 1 EDTA, 10 $NaHP_2O_7 \cdot 10H_2O$ pyrophosphate, 10 β-glycerophosphate, 10 NaF, and 0.3% CHAPS detergent (pH 7.5 adjusted using KOH) supplemented with protease inhibitor (1:200) and phosphatase 2/3 inhibitors (1:100). A 10% acrylamide get was used for mtCK while all other proteins were resolved using a 12% acrylamide gel. All gels were transferred onto 0.2 μm low fluorescence PVDF membrane (Bio-Rad, Mississauga, Canada) and blocked with Li-COR Odyssey Blocking Buffer (LI-COR, Lincoln NE) for 1 h. Membranes were then incubated with specific primary antibodies (listed below) overnight at $4°C$. A commercially available monoclonal rodent OXPHOS Cocktail (ab110413; Abcam, Cambridge, UK, 1:250 dilution) including V-ATP5A (55 kDa), III-UQCRC2 (48 kDa), IV-MTCO1 (40 kDa), II-SDHB (30 kDa), and I-NDUFB8 (20 kDa) were used to detect electron transport chain proteins. Commercially available polyclonal antibodies were used to detect VDAC 2 (32059, 33 kDa; Santa-Cruz, 1:1,000) and ANT 1 (ab180715, 32 kDa; Abcam, 1:1,000). The primary antibody for mtCK was a polyclonal serum-based primary antibody kindly provided by Dr Uwe Schlattner (Grenoble, France; 42 kDa, 1:1,000) and has been previously validated (39). After overnight primary antibody incubation, membranes were washed three times (5 min each time) in TBS-T and incubated at room temperature with appropriate fluorescent secondary antibody (LI-COR). Before detection, membranes were washed in TBS-T three times for 5 min and then imaged using infrared imaging (LI-COR CLx; LI-COR, Lincoln, NE) and quantified by densitometry (ImageJ, http://imagej.nih.gov/ij/). All images were normalized total protein assessed between 25 and 75 kDa from the same membrane stained using Amido Black total protein-stained membrane (A8181, Sigma). Western blots were at times performed on tissues from separate mice than those used for mitochondrial bioenergetics and histology, given the very small muscles at this young age, particularly in the D2.*mdx* groups, were insufficient for all analyses in this study. As such, bioenergetics data were not normalized to Western blot markers of the mitochondrial proteins outlined above.

Reduced Thiol Detection of mtCK

The redox state of mtCK thiols was assessed by labeling free thiol using IR-Dye 800CW-maleimide (Li-Cor Biotechnology, Lincoln, NE) as described previously but with slight modifications (40, 41). Briefly, quadriceps tissue was homogenized in lysis buffer (25 mM Tris-HCl pH 7.2, 150 mM NaCl, 1 mM EDTA, 1% NP-40, and 5% glycerol supplemented with a fresh protease inhibitor tablet, pH 7.2). Samples were incubated overnight at $4°C$ with IR-Dye 800CW at 100 nM/200 μg total protein. Samples were then spun through Zeba desalting columns (Exclusion size: 7 kDa MW cutoff; Thermo Fisher Scientific) twice to remove excess dye and small free thiols that could sequester the dye, and a protein concentration was determined using a BCA assay. One milligram of protein G SureBeads (Bio-Rad) was incubated with 1 μg s-mtCK

(Santa Cruz Biotechnology) for 10 min at room temperature followed by 600 µg of IR-Dye 800CW-labeled proteins, incubating overnight at room temperature. Bound proteins were then eluted with 20 mM glycine (pH 2.0) and were subjected to 10% SDS-PAGE. The gels were scanned using infrared imaging (LI-COR CLx) and quantified by densitometry (ImageJ). In this assay [essentially macroscale ALISA (42)], target-specific redox state is calculated as (IR-MAL/Total target), with total mtCK being determined via immunoblot. An increase in reversible cysteine oxidation would manifest as a loss of IR-MAL signal.

Statistics

Results are expressed as means ± SD with the level of significance established as $P < 0.05$ for all statistics. Before statistical analyses, outliers were omitted in accordance with ROUT testing (Q = 0.5%) and then tested for normality using a D'Agostino–Pearson omnibus normality test (GraphPad Prism Software, La Jolla, CA). State III respiration and mH_2O_2 were analyzed using a two-way ANOVA followed by uncorrected Fisher LSD post hoc testing when appropriate given the risk for false discovery rate is very low with a three-group design (43, 44). For all other data, statistical differences were analyzed using a one-way ANOVA (or Kruskal-Wallis for nonparametric results) between all three groups followed by uncorrected Fisher LSD or uncorrected Dunn's test (when nonparametric) post hoc analyses where appropriate. To assess creatine sensitivity in bioenergetic measurements, a two-way ANOVA within groups was applied to data collected at 100 and 500 µM ADP were examined given that 25 µM and 5 mM ADP are less sensitive to creatine.

■ RESULTS

Olesoxime Preserves Mitochondrial Bioenergetics in a Creatine-Dependent Manner

To study the effect of Olesoxime on mitochondrial bioenergetics, we determined mitochondrial respiration (a measure of oxidative phosphorylation) and H_2O_2 generation (a product of electron slip from the electron transport chain) in permeabilized fiber bundles of three experimental groups: wild-type mice (WT), D2.*mdx* mice (D2.*mdx*), and D2.*mdx* mice treated with Olesoxime for 18 days (Olesoxime). We designed in vitro assays that distinguish two different pathways of energy transfer between mitochondria and cytoplasm (Fig. 1): respiratory stimulation by either ADP alone or a combination of ADP and creatine. The latter creatine-stimulated respiration accelerates intramitochondrial recycling of ADP and the export of phosphocreatine, an energy-rich intermediate that is more highly concentrated and diffusible as compared to ADP (45–51). As the effect of creatine and mitochondrial respiration, in general, depend on ADP concentration, the primary signal of cellular energy turnover, we also analyzed a range of ADP concentrations.

In quadriceps from D2.*mdx* mice (Fig. 2), ADP-stimulated respiration driven by pyruvate/malate (NADH, Complex I) was attenuated in both creatine-independent ($P = 0.053$) and -dependent conditions ($P < 0.05$; Figs. 2, *A* and *B*) when assessed between groups. Improvements to creatine-dependent respiration were still noted after additional respiratory

stimulation with 20 mM succinate (representing Complex I + II, Supplemental Fig. S1, *A* and *B*). Olesoxime partially preserved respiration, but only in creatine-dependent conditions ($P < 0.05$; Fig. 2*B*; Supplemental Fig. S1*B*). We then directly compared the creatine-independent and -dependent condition in each experimental group (statistics assessed between these two conditions), a parameter defined here as creatine sensitivity. Such creatine sensitivity (i.e., increased respiration with creatine) was detected in WT ($P < 0.05$; Fig. 2*C*), lost in D2.*mdx* (Fig. 2*D*) but partially restored by the addition of Olesoxime ($P < 0.05$; Fig. 2*E*).

We then analyzed mH_2O_2 generation in quadriceps with succinate as substrate (allowing for reverse electron transfer through Complex I). No differences occurred between D2.*mdx* and WT (Fig. 2, *F* and *G*), whereas Olesoxime in creatine-independent conditions increased mH_2O_2 relative to WT. However, the pattern of creatine sensitivity was similar to mitochondrial respiration: attenuation of mH_2O_2 generation by creatine (51) in WT ($P < 0.05$; Fig. 2*H*) was lost in D2.*mdx* (Fig. 2*I*) but rescued by Olesoxime ($P < 0.05$; Fig. 2*J*). When using pyruvate/malate as substrates (forward electron flow through Complex I), mH_2O_2 generation increased in D2.*mdx* compared with WT ($P < 0.05$; Supplemental Fig. S2, *A* and *B*), and this increase was partially attenuated by Olesoxime ($P < 0.05$), but only in presence of creatine.

We then repeated the same analyses for diaphragm muscle (Fig. 3). As in quadriceps, D2.*mdx* diaphragm showed attenuated ADP-stimulated respiration in both creatine-independent and -dependent conditions ($P < 0.05$; Fig. 3, *A* and *B*), which was rescued by Olesoxime only in the presence of creatine ($P < 0.05$; Fig. 3*B*). This pattern seen with pyruvate/malate as substrate did not reach significance when including additional succinate (Supplemental Fig. S1, *C* and *D*). However, creatine nonetheless stimulated respiration in all groups as measured by the creatine sensitivity index ($P < 0.05$; Fig. 3, *C–E*). Generation of mH_2O_2 in diaphragm was similar to quadriceps. Specifically, in either creatine condition, there was no difference between experimental groups with succinate as substrate (Fig. 3, *F* and *G*), whereas there was an increase in D2.*mdx* and Olesoxime groups with pyruvate/malate as substrates ($P < 0.05$; Supplemental Fig. S2, *C* and *D*). Importantly, the pattern of creatine sensitivity was again the same as in quadriceps: attenuation of mH_2O_2 generation by creatine in WT ($P < 0.05$; Fig. 3*H*) was lost in D2.*mdx* (Fig. 3*I*) but rescued by Olesoxime ($P < 0.05$; Fig. 3).

We next determined whether the reduced mitochondrial creatine sensitivity in D2.*mdx* and its preservation by Olesoxime were related to altered protein levels of key components in mitochondrial energy transfer (see Fig. 1). No differences were noted in the contents of specific subunits within Complexes I-V except for reductions within Complex III in quadriceps for both D2.*mdx* and Olesoxime relative to WT (Fig. 4, *A* and *B*). Reductions in VDAC2 and ANT1 isoforms in D2.*mdx* quadriceps and ANT1 in the diaphragm ($P < 0.05$) were unaltered by Olesoxime (Supplemental Fig. S3, *B–E*). Mitochondrial creatine kinase (mtCK) was lower in D2.*mdx* and Olesoxime versus WT in quadriceps ($P < 0.05$; Fig. 4*C*) but not diaphragm (Fig. 4*D*), and again unaltered by Olesoxime. Noting that mtCK is inhibited by reactive oxygen

species (53), we then assessed the relative amount of exposed cysteine residues in the reduced state on immunoprecipitated mtCK (see MATERIALS AND METHODS). Cysteine oxidation is the first oxidative modification that occurs in the mtCK octamer on the onset of oxidative stress (49). However, no differences were seen for mtCK thiol redox state in any group in quadriceps ($P > 0.05$; Supplemental Fig. S3A), suggesting differences in creatine sensitivity (Fig. 2) were not due to redox modifications of this complex. Assessments were not performed in the diaphragm given tissue limitations at this young age in the D2.mdx model.

Reduced and Total Glutathione Are Increased in D2.mdx Diaphragm but Are Not Affected by Olesoxime

To determine whether alterations in creatine sensitivity during mH_2O_2 affected global cellular redox conditions, we assessed glutathione equilibria in each group. In quadriceps, there were no differences in total reduced GSH (Fig. 5A), oxidized GSSG (Fig. 5B), their equilibria (GSH: GSSG; Fig. 5C) or their sum (total glutathione; Fig. 5D). In diaphragm, reduced GSH ($P < 0.05$; Fig. 5E) and total glutathione ($P < 0.05$; Fig. 5H) were elevated in D2.mdx consistent with past reports of possible compensations in

redox buffering in mdx mice (13, 14). Olesoxime tended to preserve the WT levels of reduced GSH ($P = 0.061$; Fig. 5E). There were no further differences in GSSG (Fig. 5F) and GSH:GSSG (Fig. 5G).

Olesoxime Does Not Alter Mitochondrial Calcium Retention Capacity nor Muscle Necrosis or Fibrosis

Prior reports suggested that Olesoxime can attenuate the formation of the permeability transition pore (mPTP) (5, 6, 21). Given excess calcium stress in dystrophic fibers is thought to trigger mPTP and apoptosis as contributors to degeneration, we next compared mitochondrial calcium retention capacity, a functional readout of mPTP, to histological measures of fiber degeneration and fibrosis. We included creatine and ADP in the assay media given both are known to regulate mPTP through an attenuation effect (53–55). In quadriceps, reductions in calcium retention capacity were noted in D2.mdx with and without Olesoxime ($P < 0.05$; Fig. 6A), which reflects an increased sensitivity of mPTP to calcium stress. However, there were no changes in caspase 3 or 9 activity (Supplemental Fig. S4, A and B), which can mediate apoptosis downstream of putative mPTP opening (56–59). This observation was
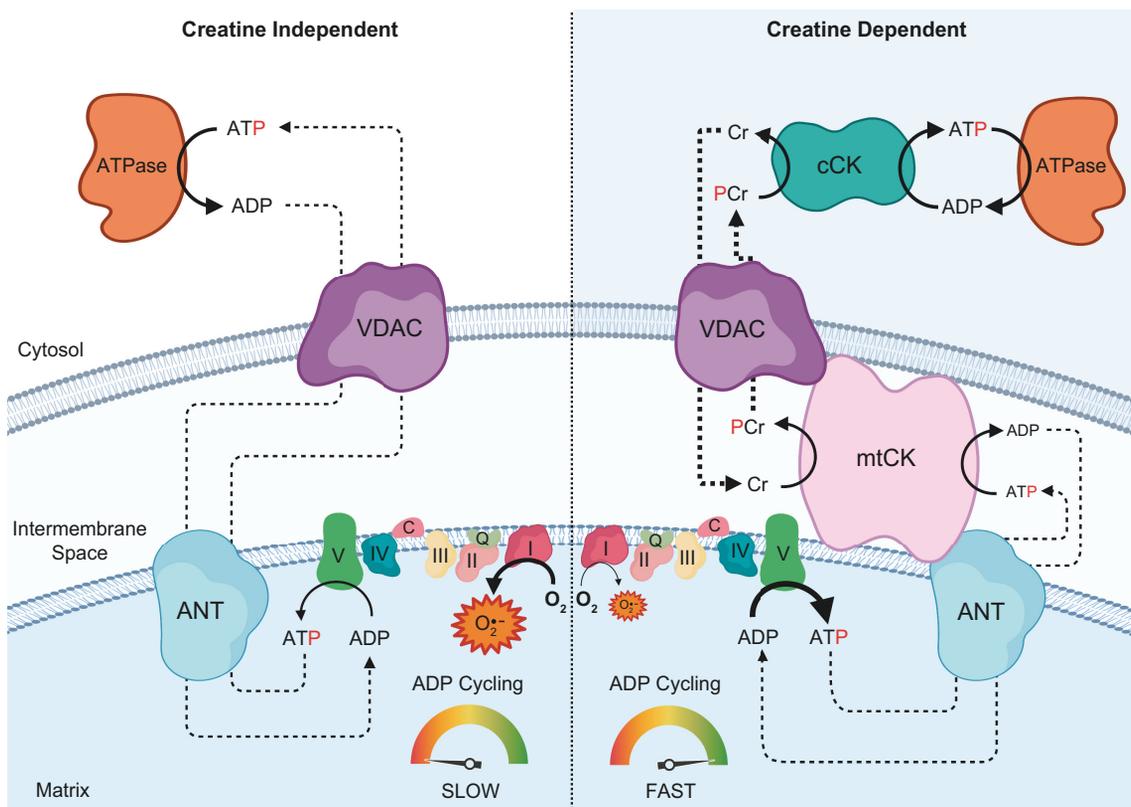

Figure 1. Schematic representation of creatine-dependent and -independent control of oxidative phosphorylation and mH_2O_2. Creatine-independent phosphate shuttling between mitochondrial and cytoplasmic compartments (*left*) occurs via ADP/ATP cycling across the voltage-dependent anion carrier (VDAC) on the outer mitochondria membrane and adenosine nucleotide translocase (ANT) on the inner membrane. Creatine-dependent phosphate shuttling (right) was facilitated by mitochondrial creatine kinase (mtCK) whereby the transfer of phosphate from ATP to Cr in the intermembrane space produces phosphocreatine (PCr) and ADP. PCr is then exported through VDAC into the cytosol and ADP is shuttled back into the matrix via ANT. The relatively faster diffusion kinetics and higher cellular concentrations of PCr/Cr vs. ATP/ADP combined with a reduction of diffusion distances for the latter allow for increased energy turnover. Electrons may slip and interact with nearby oxygen forming a superoxide radical ($O_2^{\bullet-}$). The relative size between the creatine-independent (*left*) and -dependent (*right*) refers to the increased production of superoxide in the absence of creatine. C, cytochrome C; Q, coenzyme Q. Figure based on discoveries reported in Refs. 45–51. Figure was created with BioRender.com.
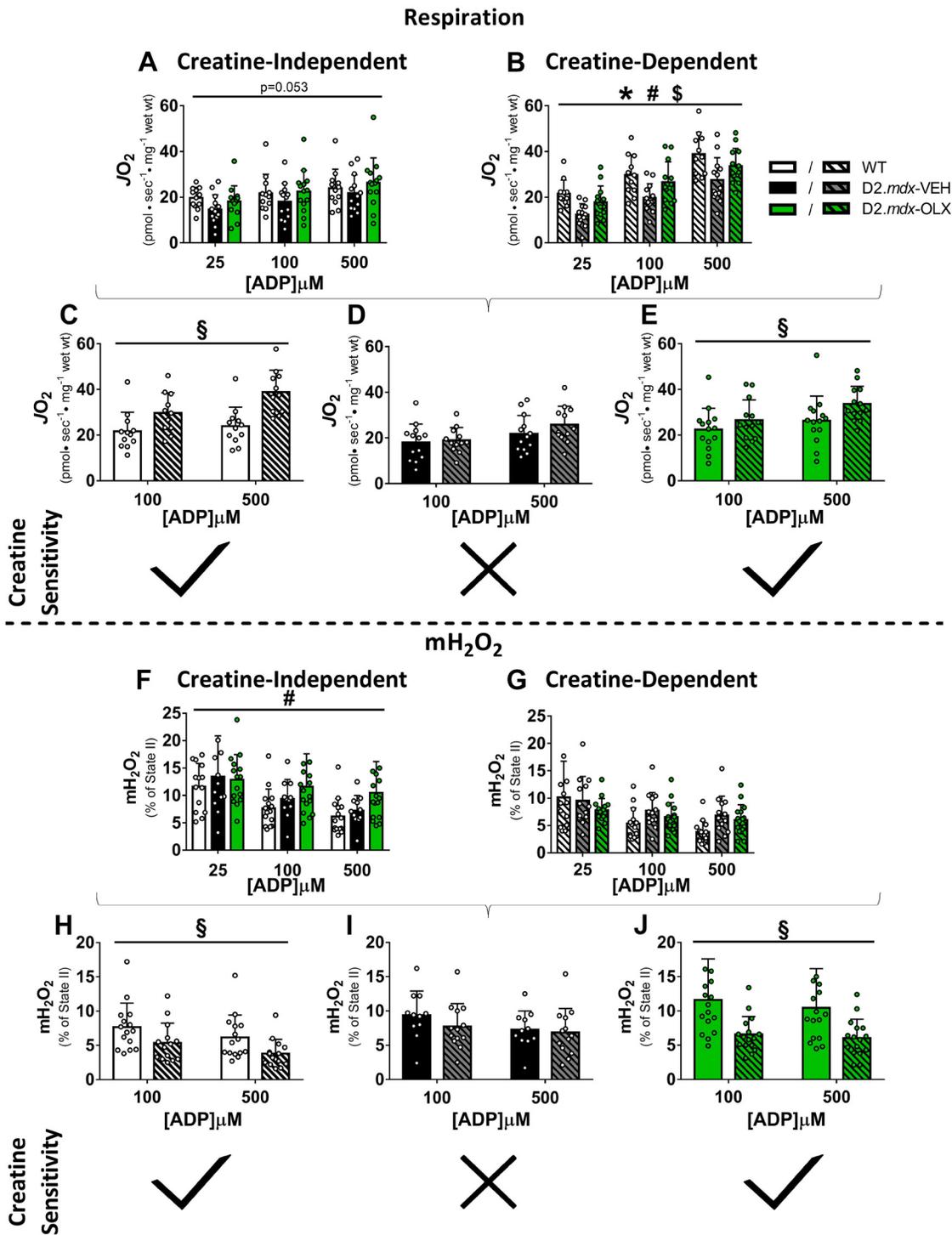
Figure 2. In quadriceps, Olesoxime preserves creatine sensitivity of mitochondrial respiration and mitochondrial H_2O_2 emission. *A* and *B*: complex I-supported respiration stimulated by NADH generation through 5 mM pyruvate and 2 mM malate (NADH) in permeabilized muscle fibers across a range of ADP concentrations that represent increasing states of metabolic demand: 25 μM [resting muscle (30)]; 100 μM [high-intensity exercise (52)], and 500 μM (supramaximal) in both the absence and presence of 20 mM creatine. *C–E*: mitochondrial respiratory sensitivity to creatine (data replotted from *A* and *B*) at ADP concentrations that are subject to control by creatine (47) as done previously (14, 18). *F–J*: similar analyses were performed to assess the ability of creatine to enhance ADP's effect on attenuating mH_2O_2 supported by 10 mM succinate ($FADH_2$). Note that this stimulates Complex II but also leads to reverse electron flow through Complex I known to generate reactive oxygen species. *$P < 0.05$ WT vs. D2.*mdx*-VEH; #$P < 0.05$ WT vs. D2.*mdx*-OLX; $$P < 0.05$ D2.*mdx*-VEH vs. D2.*mdx*-OLX. §$P < 0.05$ Cr vs. No Cr condition. Data are shown as means ± SD, $n = 10$–14. OLX, Olesoxime; VEH, vehicle; WT, wild type.
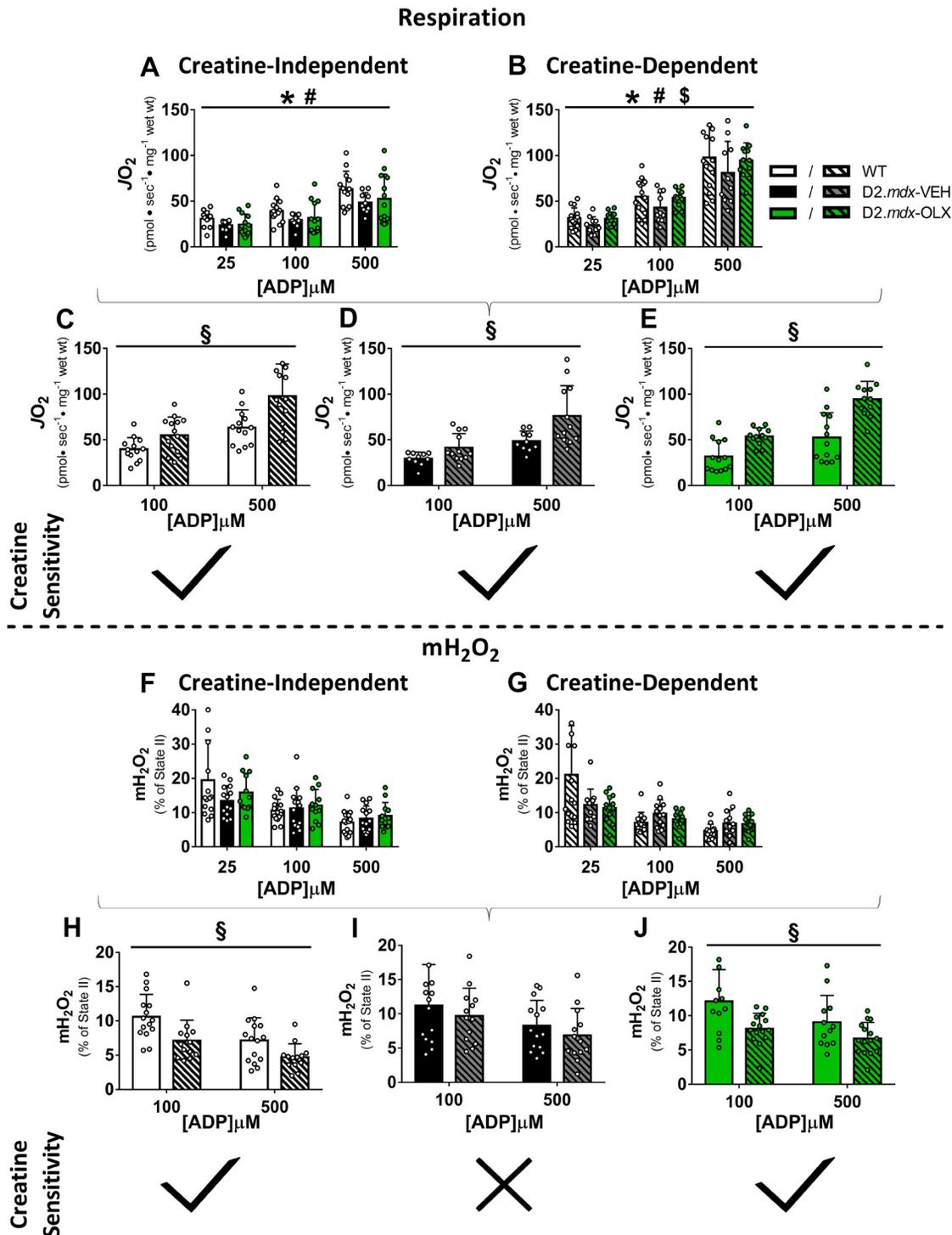
Figure 3. In diaphragm, Olesoxime preserves mitochondrial creatine-dependent respiration and preserves creatine sensitivity during mitochondrial H₂O₂ emission. *A* and *B*: as in Fig. 2, complex I-supported respiration stimulated by NADH generation through 5 mM pyruvate and 2 mM malate in permeabilized muscle fibers across a range of ADP concentrations that represent increasing states of metabolic demand: 25 µM [resting muscle (30)]; 100 µM [high-intensity exercise (52)] and 500 µM (supramaximal) in both the absence and presence of 20 mM creatine. *C–E*: mitochondrial respiratory sensitivity to creatine (data replotted from *A* and *B*) at ADP concentrations that are subject to control by creatine (47) as done previously (14, 18). *F–J*: similar analyses were performed to assess the ability of creatine to enhance ADP's effect on attenuating mH₂O₂ supported by 10 mM succinate (FADH₂). Note that this stimulates Complex II but also leads to reverse electron flow through Complex I known to generate reactive oxygen species. *$P < 0.05$ WT vs. D2.*mdx*-VEH; #$P < 0.05$ WT vs. D2.*mdx*-OLX; $$P < 0.05$ D2.*mdx*-VEH vs. D2.*mdx*-OLX. §$P < 0.05$ Cr vs. No Cr condition. Data are shown as means ± SD, *n* = 10–14. OLX, Olesoxime; VEH, vehicle; WT, wild type.
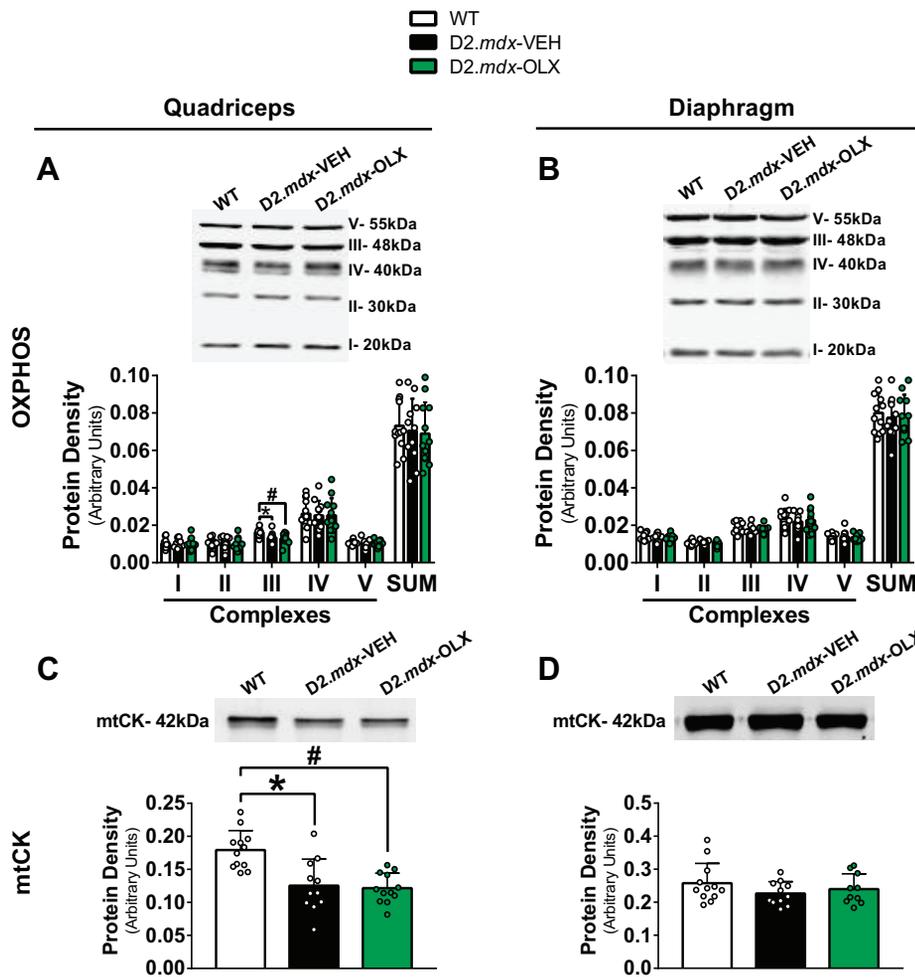
Figure 4. Olesoxime did not alter contents of electron transport system proteins or mitochondrial creatine kinase in quadriceps and diaphragm. Subunits of Complexes I, II, III, IV, and V (ATP Synthase; *A* and *B*) and (*C* and *D*) mtCK were assessed by western blot. *$P <$ 0.05 WT vs. D2.*mdx*-VEH; #$P <$ 0.05 WT vs. D2.*mdx*-OLX. Data are shown as means ± SD, n = 10–12. OLX, Olesoxime; VEH, vehicle; WT, wild type.

related to increased fiber degeneration and fibrosis ($P <$ 0.05; Fig. 6, *B–E*). There was no effect of Olesoxime on these measures. In diaphragm, there were no differences in calcium retention capacity consistent with prior observations that this measure of mPTP is altered in a muscle-specific manner in young D2.*mdx* mice (14). Likewise, fiber degeneration and fibrosis were present in D2.*mdx* diaphragm ($P <$ 0.05) but were not altered by Olesoxime (Fig. 6, *G–J*). There were no changes in caspase 3 or 9 activity in diaphragm (Supplemental Fig. S3, *D* and *E*) or caspase 8, which is activated by extracellular stressors and can influence mPTP (60).

Olesoxime Alters Cross-Sectional Area and Distribution in a Fiber Type- and Muscle-Specific Manner

Muscle atrophy is a hallmark characteristic of DMD. Using antibodies specific for myosin heavy chain isoforms (Fig. 7, *A, B, D,* and *E*), we next determined the response of specific fibers to Olesoxime. In quadriceps, atrophy was not observed in any fiber type in D2.*mdx* in contrast to a prior report at this same age and muscle showed an increased cross-sectional area averaged over all fiber types (14). Olesoxime decreased cross-sectional area of Type I fibers in quadriceps ($P <$ 0.05; Fig. 7*B*). The proportion of type IIA fibers (%) was elevated in D2.*mdx* ($P <$ 0.05), whereas Olesoxime lowered distribution in I and IIA fibers

($P <$ 0.05; Fig. 7*C*). In diaphragm, D2.*mdx* showed lower cross-sectional areas in IIA and IIX fibers with the latter being preserved by Olesoxime ($P <$ 0.05; Fig. 7, *D* and *E*). There were no differences in fiber type distribution between groups (Fig. 7*F*).

Olesoxime Improves Recovery from Fatigue in Diaphragm

We next assessed aspects of muscle force given dystrophin mutations cause severe muscle weakness, which severely compromises the quality of life in DMD. Diaphragm muscle strips were subjected to a series of stimulation protocols (Fig. 8*A*) using force-frequency (Fig. 8*B*) followed by determination of fatigue (Fig. 8*C*) and recovery from fatigue (Fig. 8*D*). Olesoxime improved recovery of force across 15 min of assessments during recovery ($P <$ 0.05). Due to technical limitations, assessments were not performed in the quadriceps.

Olesoxime Improves Specific Markers of Muscle and Bone Health

Finally, we determined some clinically relevant measures of muscle and bone quality. Using serum creatine kinase as a marker of muscle damage, we found that increases in D2.*mdx* mice were robustly reduced by Olesoxime ($P <$ 0.05; Fig. 9*A*). Likewise, Olesoxime
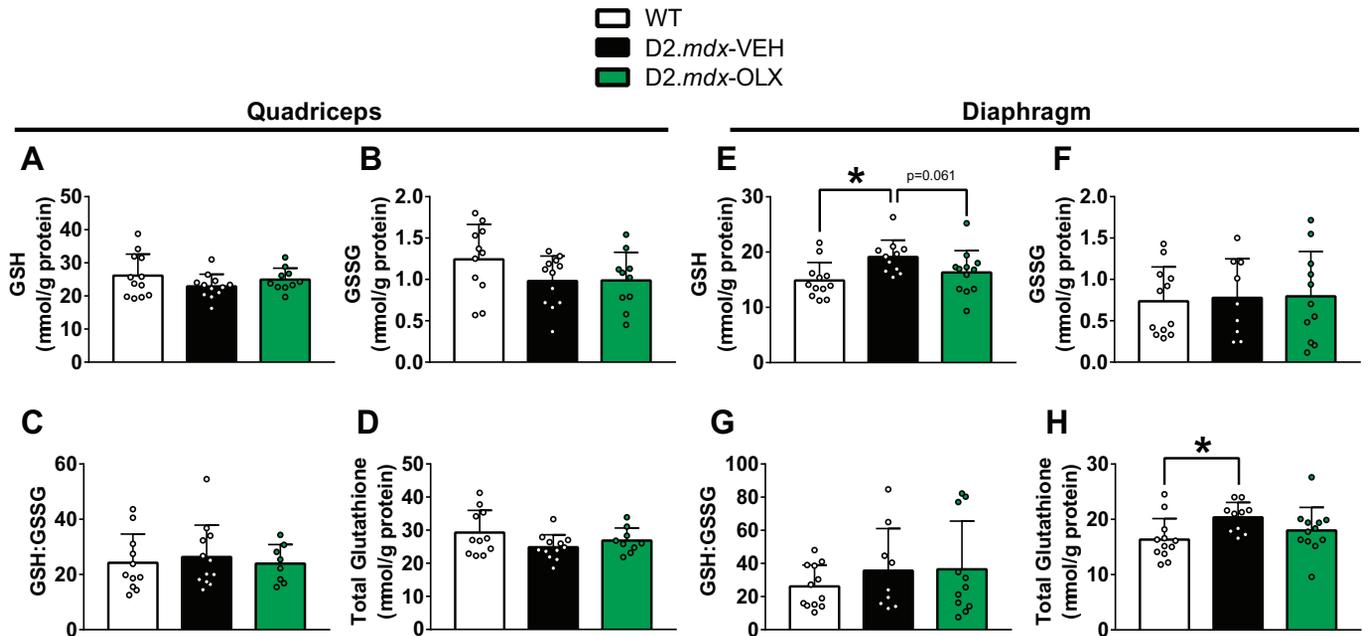
Figure 5. Glutathione assessments in quadriceps and diaphragm. *A–H*: glutathione was assessed in its reduced (GSH) and oxidized forms (GSSG), as an equilibria (GSH:GSSG) and as total content (GSH + 2xGSSG) in both quadriceps and diaphragm. *$P < 0.05$ WT vs. D2.*mdx*-VEH. Data are shown as means ± SD, $n = 8$–12. OLX, Olesoxime; VEH, vehicle; WT, wild type.

modestly improved voluntary cage hang-time ($P < 0.05$; Fig. 9B). Reductions in voluntary running wheel distance (Fig. 9C), grip strength (Fig. 9D), and distance explored in an open field ($P < 0.05$; Fig. 9E) were observed in D2.*mdx* but were unaltered by Olesoxime. We then used 3-dimensional microCT scans to assess aspects of body volume and composition. Modest reductions in whole body volume at this early disease stage were prevented by Olesoxime ($P < 0.05$; Fig. 9F). Likewise, Olesoxime modestly increased hindlimb muscle volume ($P < 0.05$; Fig. 9G). There was a general increase in whole body lean volume measures, which includes muscle and visceral organs excluding lung that was accentuated by Olesoxime ($P < 0.05$; Fig. 9H). We also assessed bone volume given reductions in bone mass are recognized as a risk in DMD. Intriguingly, reductions in hindlimb bone volume in D2.*mdx* were partially prevented by Olesoxime ($P < 0.05$; Fig. 9I). Olesoxime did not alter adipose tissue volumes or other assessed volumetric parameters (Supplemental Table S1).

DISCUSSION

Recent reports indicate that several mitochondrial stress responses occur within the first few days of age in D2.*mdx* mice (14, 18, 61) suggesting that mitochondria may be a secondary contributor to myopathy in DMD. Here, we demonstrated that the mitochondrial-enhancing compound Olesoxime can preserve *1*) creatine-sensitive mitochondrial functions, in particular Complex I-supported creatine-stimulated respiration and attenuation of H_2O_2 generation, *2*) recovery from muscle fatigue, and *3*) different clinically relevant markers of muscle quality by 4 wk of age. An overall heterogeneous effect of Olesoxime on

respiratory and limb muscle quality also suggests mitochondrial influences on myopathy varies across muscle types. Thus, mitochondrial stress may have distinct influences on the progression of myopathy in DMD depending on age and muscle type.

Possible Mechanisms of Olesoxime

Alterations in oxidative phosphorylation and generation of reactive oxygen species have been described for D2.*mdx* muscle (14, 17, 18) and other dystrophin-deficient models (4). For analyzing these parameters in more detail in our study, we carefully considered two different pathways of energy exchange between mitochondria and the cytoplasm: ADP/ATP versus creatine/phosphocreatine cycling. In both pathways, high-energy phosphate is shuttled from the matrix to the cytoplasm albeit through different carriers (adenylates vs. creatine) and at different rates (creatine/phosphocreatine being faster).

By reconstituting these pathways in vitro through the exclusion or inclusion of creatine in the respirometric assay media as performed previously (14, 28, 30, 32, 62–65), we discovered that the ability of creatine to stimulate coupled respiration is lost in D2.*mdx* quadriceps and is consistent with our previous observations in multiple muscle types in this model (14, 18). This mitochondrial creatine insensitivity was reversed following treatment with Olesoxime (Fig. 2, *C–E*), which is a mechanism not previously reported for this compound. Finally, the loss of creatine sensitivity in D2.*mdx* was not observed in the diaphragm in contrast to our prior report (14), which might be related to a possible variability in the dynamic remodeling of a muscle occurring over days to weeks at this young age. Olesoxime did not increase mtCK abundance or decrease mtCK oxidation in D2.*mdx* quadriceps. However,
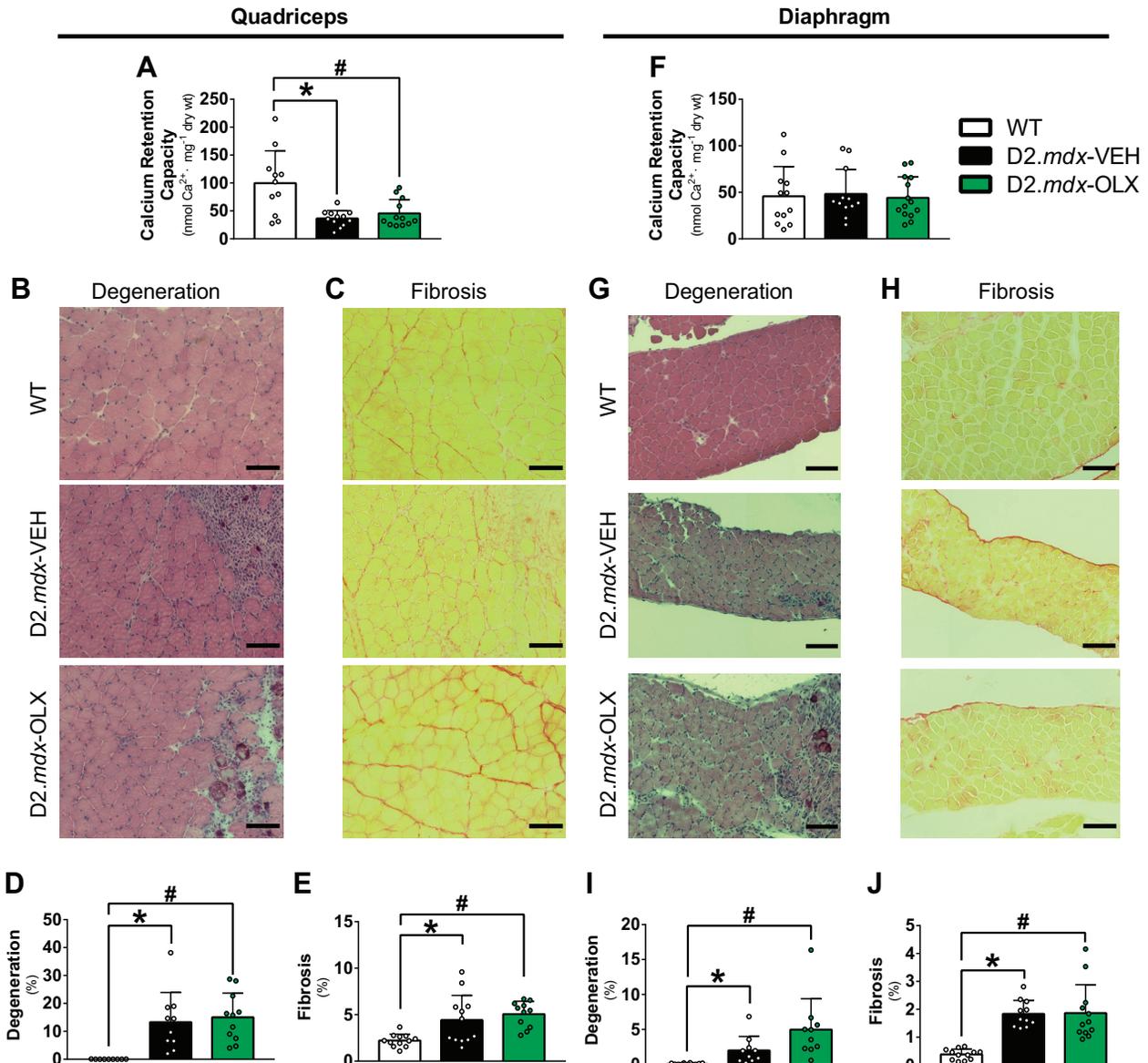
Figure 6. Increases in mitochondrial permeability transition pore, fiber degeneration, and fibrosis in quadriceps and diaphragm of D2.*mdx* are not altered by Olesoxime. *A*: in quadriceps, calcium retention capacity was assessed spectrofluorometrically by titrating calcium permeabilized fibers until the mPTP was triggered. *B–E*: histological assessments of muscle fiber degeneration and fibrosis were performed with hematoxylin & eosin (H&E) and picrosirius red, respectively. Representative images were obtained with ×20 magnification. *F–J*: similar measures were performed in diaphragm muscle. *$P < 0.05$ WT vs. D2.*mdx*-VEH; #$P < 0.05$ WT vs. D2.*mdx*-OLX. Scale bar = 100 μm. Data are shown as means ± SD, n = 9–14. OLX, Olesoxime; VEH, vehicle; WT, wild type.

mtCK oxidation could be evaluated with multiple thiol labeling methodologies given the technique used in the present study detects reduced thiols that exist in high abundance and may be less sensitive than thiol oxidation assessments such as the recently developed ALISA (42). It is also possible that other elements of the creatine/phosphocreatine pathway (Fig. 1) are targeted by the drug. These include the assembly of octameric mtCK within the proteolipid complex as shown in Fig. 1 (49) or the permeability of the outer membrane VDAC pore. The latter is a likely candidate when considering the biological activity of Olesoxime as addressed below. Lastly, although we report changes in creatine-dependent respiration supported by Complex I, future work could consider whether

these creatine responses are conserved across multiple substrate inputs.

Strikingly, mitochondrial H_2O_2 generation in both quadriceps and diaphragm showed the same creatine sensitivity pattern and rescue by Olesoxime as seen for quadriceps respiration. H_2O_2 is the major oxidant generated by mitochondria (66, 67) and elevations have been reported at this age in D2.*mdx* mice in association with early myopathy (14, 17, 18). Key to the design of our in vitro assays was the recognition that the rate of mH_2O_2 is inversely proportional to the degree of coupled respiration (68). We stimulated respiration across a range of ADP concentrations from low to high in presence or absence of creatine to include physiologically relevant conditions. As a key finding of our study, the observed
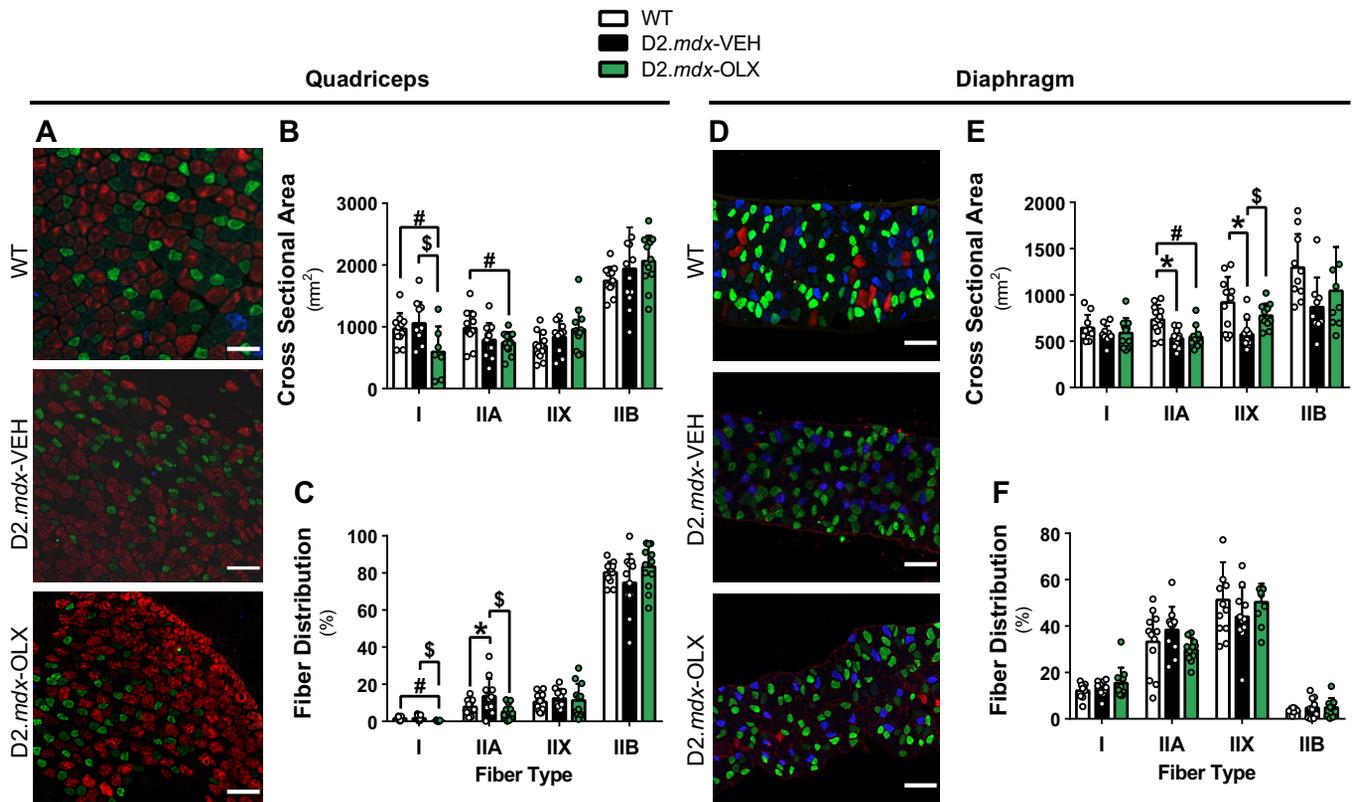
Figure 7. Divergent effects of Olesoxime on muscle fiber type size and distribution in quadriceps and diaphragm of D2.*mdx*. *A*: representative images of quadriceps muscle fibers stained for specific isoforms of myosin heavy chain, where blue are type I fibers, green are IIA fibers, black are IIX fibers and red are IIB fibers. *B* and *C*: images were quantified to calculate cross-sectional area and distribution of myosin heavy chain-specific fibers. *D–F*: similar measures were repeated in diaphragm fibers. *P < 0.05 WT vs. D2.*mdx*-VEH; #P < 0.05 WT vs. D2.*mdx*-OLX; $P < 0.05 D2.*mdx*-VEH vs. D2.*mdx*-OLX. Scale bar = 100 μm. Data are shown as means ± SD, n = 10–12. OLX, Olesoxime; VEH, vehicle; WT, wild type.

creatine sensitivity patterns suggest that loss of creatine sensitivity occurring in D2.*mdx* mice and its rescue by Olesoxime is a general feature. This evidently raises the question as to how Olesoxime regulates creatine sensitivity.

Olesoxime seems to exert its biological activity by accumulating in mitochondrial membranes and binding to the outer membrane proteins VDAC and peripheral benzodiazepine receptor (TSPO) on the outer mitochondrial membrane TSPO (69). Based on this interaction with VDAC, some initial reports suggested inhibition of the inner membrane mPTP as a major mechanism of Olesoxime (5–8). However, there is now consensus that VDAC is not always a mPTP component. We did not observe an effect of Olesoxime on mitochondrial calcium retention capacity, the standard assay for mPTP calcium sensitivity, consistent with a previous report (6). Such calcium stress was chosen as a mPTP inducer (70, 71) since dystrophin-deficient muscle shows cytosolic calcium overload (72, 73), which may cause mitochondrial stress (4). Although we cannot exclude attenuation of mPTP by mechanisms not detectable with our calcium retention assay, it seems more likely that Olesoxime affects calcium homeostasis or cytochrome c release as found in other studies (5, 21) independently of mPTP. By enriching in the mitochondrial outer membrane and interacting with VDAC and TSPO, Olesoxime may more directly control the permeability of the outer membrane for small molecules like calcium (69)

and creatine/phosphocreatine, or cholesterol exchange and membrane fluidity. Additionally, Olesoxime may also affect the assembly of larger Bax pores which allows for efflux of macromolecules like cytochrome c (74, 75). Thus, our findings add new insight into the mechanisms by which Olesoxime preserves mitochondrial bioenergetics and proposes alternative stress-related mechanisms.

Mitochondrial Relationships to Myopathy in *D2.mdx* Muscle

Our study suggests that preservation of mitochondrial creatine sensitivity is linked to muscle quality in D2.*mdx* mice. Although several markers showed modest improvements, the more notable responses to Olesoxime included a robust reduction in circulating serum creatine kinase—a marker of muscle injury—and improved recovery from fatigue in diaphragm. Although we were unable to perform force assessments in quadriceps due to technical limitations, these findings provide a foundation to further explore the importance of mitochondrial creatine functions in regulating muscle function and contributing to weakness in dystrophin-deficient muscle. Not all measures of muscle quality improved with Olesoxime, but this may not be surprising given mitochondrial stress is secondary to dystrophin deficiency and will not be the only contributor to myopathy given the known inflammatory, cytoskeletal, calcium, and other stressors that arise in this disorder. Although speculative, an
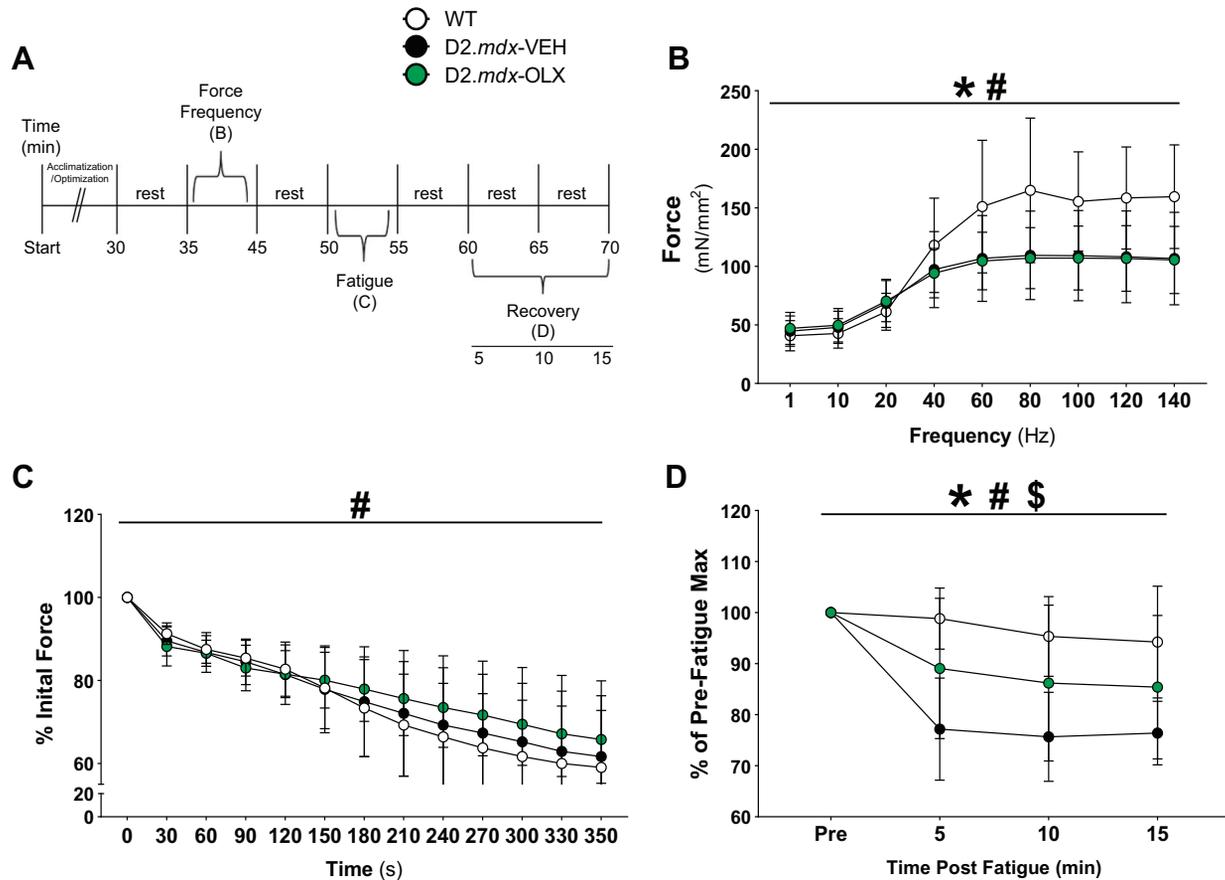
Figure 8. Olesoxime improves recovery of force following fatigue in diaphragm. *A*: muscle force was assessed using a series of force-frequency, fatigue, and recovery protocols. *B*: force-frequency was assessed in vitro using isolated diaphragm strips followed (1–140 Hz for 0.2 ms) by (*C*) a fatiguing protocol (70 Hz for 350 ms every 2 s for 5 min). *D*: single stimulations were used to assess recovery from fatigue. *$P < 0.05$ WT vs. D2.*mdx*-VEH; #$P < 0.05$ WT vs. D2.*mdx*-OLX; $$P < 0.05$ D2.*mdx*-VEH vs. D2.*mdx*-OLX. Data are shown as means ± SD, $n = 9$–12. OLX, Olesoxime; VEH, vehicle; WT, wild type.

additional consideration for future directions includes the influence of mitochondrial metabolism in cell types that modify muscle remodeling including fibroblasts, fibroadipogenic precursors, and macrophages (see Ref. 4 for perspectives), particularly with longer term treatments throughout disease progression. Nevertheless, the early improvements with this short-term treatment regimen seen in the present investigation indicate that mitochondrial stress likely contributes to the early myopathy in D2.*mdx* muscle.

In this regard, the 4-wk-old mice examined in this study capture a time of dynamic development as mice mature. The interaction between both developmental and disease influences on mitochondria will inevitably be complex, with the reciprocal relationship being one of many determinants of muscle quality. Nonetheless, this early age provides relevant context given myopathy develops in young children with DMD (1, 76). The heterogeneous relationship between altered mitochondrial creatine metabolism and muscle quality in the current study also provides a foundation for exploring other mitochondrial-enhancing therapies across a range of doses and treatment durations across stages of disease development using muscle-specific comparisons.

An additional point of interest pertains to the mitochondrial calcium retention capacity measures. In vehicle-treated mice, calcium retention capacity was reduced in the quadriceps but not in the diaphragm compared to wild-

type consistent with our previous report (14). This finding demonstrates that mitochondrial stress responses in one muscle do not necessarily predict the response in another muscle. Such muscle-specific mitochondrial responses to dystrophin mutations are an intriguing opportunity to understand the precise mechanisms by which stress signals differ between muscles or whether mitochondrial resilience to a given stress signal is heterogeneous across the musculature (see Ref. 4 for perspective). The regulation of mitochondrial calcium cycling is of course complex and includes additional regulators not considered in this study including mitochondrial calcium uniporters. In this regard, 4-wk-old C57Bl10.*mdx* mice demonstrate increases in MCUb (the inactive channel subunit of the uniporter), which lowered the ratio of MCU/MCUb (77) and is thought to be a metric that regulates the mitochondrial calcium transport kinetics. Our observations of muscle-specific sensitivity or resilience to exogenous calcium stresses in vitro support future considerations of how MCU responses in this disease might contribute to this heterogeneity.

From a broader perspective, the potential efficacy of targeting mitochondria to treat muscle weakness in DMD warrants further focus, particularly with consideration of translation from preclinical models to clinical trials. For example, the quinone electron shuttling drug Idebenone improved cardiac
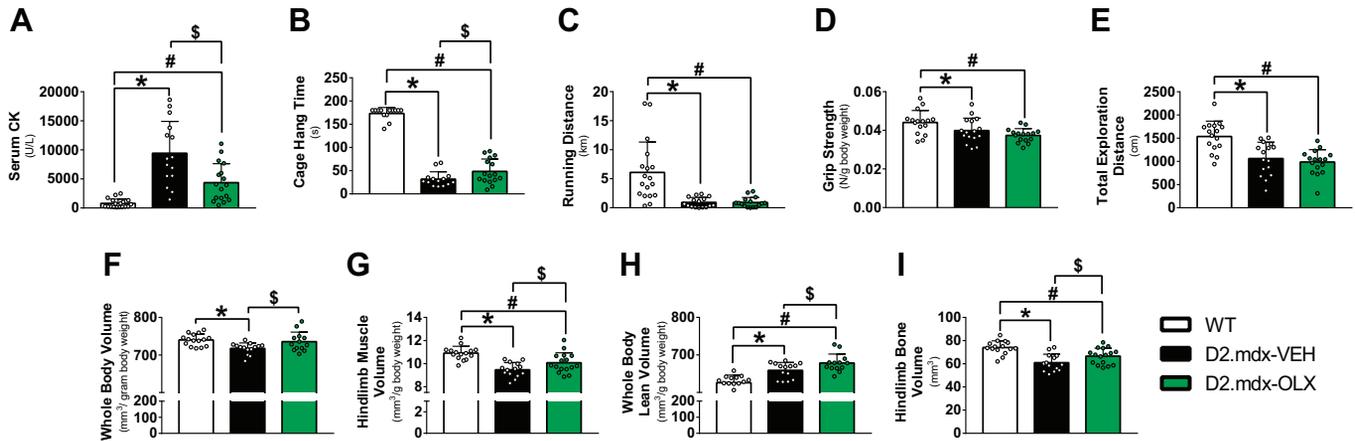
Figure 9. Olesoxime improves specific markers of muscle health and bone volume. *A*: serum creatine kinase (CK) was used as a clinically relevant marker of muscle damage. *B*: voluntary hang-time was assessed with mice hanging to an inverted cage lid over a soft pad with assessments stopped at 180 s. *C*: voluntary running wheel distance was assessed over 24 h. *D*: grip strength was assessed using a grip strength meter and normalized to body weight. *E*: mice were placed in open-field container and video recordings were taken over 6 min to quantify voluntary total exploration distance. 3-dimensional microCT scans were used to assess (*F*) whole body muscle volume, (*G*) hindlimb muscle volume, (*H*) whole body lean volume, and (*I*) hindlimb bone volume. *$P < 0.05$ WT vs. D2.*mdx*-VEH; #$P < 0.05$ WT vs. D2.*mdx*-OLX; $$P < 0.05$ D2.*mdx*-VEH vs. D2.*mdx*-OLX. Data are shown as means ± SD, n = 13–18. OLX, Olesoxime; VEH, vehicle; WT, wild type.

function and exercise performance in a mouse model of DMD, which was subsequently shown to also improve cardiac and respiratory function in an initial clinical trial of people with DMD (78, 79). However, subsequent clinical trials proved unsuccessful (NCT 02814019) for reasons that are not fully understood. These early attempts at targeting mitochondria demonstrate that mitochondria could be a potential therapeutic target in DMD but that additional consideration of pharmacological and biological factors influencing the translation of findings from preclinical models to humans will be important for continued progress in developing mitochondrial therapeutics. Nonetheless, the results from the present investigation identify mitochondrial creatine sensitivity linked to respiration and mH_2O_2 attenuation as a new direction to for continued research in preclinical research.

Conclusions

This study examined the efficacy of early, short-term administration of Olesoxime in the treatment of D2.*mdx* mice. In the dystrophin-deficient muscle, Olesoxime preserved mitochondrial creatine sensitivity in terms of creatine-stimulated respiration and attenuated mH_2O_2 and improved markers of muscle function and quality. This suggests that mitochondria contribute to myopathy in DMD, albeit to a degree that may depend on age and muscle type and the relative influence of other disease stressors. However, Olesoxime did not improve mitochondrial calcium retention capacity, questioning the role of the drug in altering calcium-induced mPTP. Rather, the effect of the compound on creatine sensitivity suggests regulation of outer membrane permeability or stability of the mtCK proteolipid complex. Future studies in D2.*mdx* mice should address the mechanism underlying creatine sensitivity and the effects of longer-term Olesoxime treatment on mitigation of oxidative stress and improved creatine sensitivity as a new direction in developing prospective mitochondrial-enhancing therapies for Duchenne muscular dystrophy.

SUPPLEMENTAL DATA

Supplemental Figs. S1–S4 and Supplemental Table S1: https://doi.org/10.6084/m9.figshare.20512263.v2.

DATA AVAILABILITY

Data will be made available upon reasonable request.

DISCLOSURES

No conflicts of interest, financial or otherwise, are declared by the authors.

AUTHOR CONTRIBUTIONS

C.A.B., M.C.H., J.N.C., and C.G.R.P. conceived and designed research; C.A.B., L.J.D., P.C.T., S.G., S.N.D., F.A.R., P.T., C.A., and A.D. performed experiments; C.A.B., P.C.T., S.G., S.N.D., F.A.R., P.T., C.A., A.D., and C.G.R.P. analyzed data; C.A.B., L.J.D., M.C.H., P.C.T., S.G., F.A.R., P.T., J.N.C., J.Q., U.S., and C.G.R.P. interpreted results of experiments; C.A.B., F.A.R., and C.G.R.P. prepared figures; C.A.B., L.J.D., S.G., F.A.R., P.T., J.N.C., J.Q., U.S., and C.G.R.P. drafted manuscript; C.A.B., L.J.D., M.C.H., P.C.T., S.G., S.N.D., F.A.R., P.T., C.A., A.D., J.N.C., J.Q., U.S., and C.G.R.P. edited and revised manuscript; C.A.B., L.J.D., M.C.H., P.C.T., S.G., S.N.D., F.A.R., P.T., C.A., A.D., J.N.C., J.Q., U.S., and C.G.R.P. approved final version of manuscript.

REFERENCES

1. **Emery A.** Genetic heterogeneity in Duchenne muscular dystrophy. *Am J Med Genet* 26: 235–236, 1987. doi:10.1002/ajmg.1320260138.

2. **Hoffman EP.** The discovery of dystrophin, the protein product of the Duchenne muscular dystrophy gene. *FEBS J* 287: 3879–3887, 2020. doi:10.1111/febs.15466.

3. **Petrof BJ.** The molecular basis of activity-induced muscle injury in Duchenne muscular dystrophy. *Mol Cell Biochem* 179: 111–123, 1998. doi:10.1023/a:1006812004945.

4. **Bellissimo CA, Garibotti MC, Perry CGR.** Mitochondrial stress responses in Duchenne muscular dystrophy: metabolic dysfunction or adaptive reprogramming? *Am J Physiol Cell Physiol* 323: C718–C730, 2022. doi:10.1152/ajpcell.00249.2022.

5. **Bordet T, Buisson B, Michaud M, Drouot C, Galéa P, Delaage P, Akentieva NP, Evers AS, Covey DF, Ostuni MA, Lacapère J-J, Massaad C, Schumacher M, Steidl E-M, Maux D, Delaage M, Henderson CE, Pruss RM.** Identification and characterization of cholest-4-en-3-one, oxime (TRO19622), a novel drug candidate for amyotrophic lateral sclerosis. *J Pharmacol Exp Ther* 322: 709–720, 2007. doi:10.1124/jpet.107.123000.

6. **Bordet T, Berna P, Abitbol JL, Pruss RM.** Olesoxime (TRO19622): a novel mitochondrial-targeted neuroprotective compound. *Pharmaceuticals (Basel)* 3: 345–368, 2010. doi:10.3390/ph3020345.

7. **Clemens LE, Weber JJ, Wlodkowski TT, Yu-Taeger L, Michaud M, Calaminus C, Eckert SH, Gaca J, Weiss A, Magg JC, Jansson EK, Eckert GP, Pichler BJ, Bordet T, Pruss RM, Riess O, Nguyen HP.** Olesoxime suppresses calpain activation and mutant huntingtin fragmentation in the BACHD rat. *Brain* 138: 3632–3653, 2015. doi:10.1093/brain/awv290.

8. **Gouarné C, Giraudon-Paoli M, Seimandi M, Biscarrat C, Tardif G, Pruss RM, Bordet T.** Olesoxime protects embryonic cortical neurons from camptothecin intoxication by a mechanism distinct from BDNF. *Br J Pharmacol* 168: 1975–1988, 2013. doi:10.1111/bph.12094.

9. **Bertini E, Dessaud E, Mercuri E, Muntoni F, Kirschner J, Reid C, Lusakowska A, Comi GP, Cuisset JM, Abitbol JL, Scherrer B, Ducray PS, Buchbjerg J, Vianna E, van der Pol WL, Vuillerot C, Blaettler T, Fontoura P; Olesoxime SMA Phase 2 Study Investigators.** Safety and efficacy of olesoxime in patients with type 2 or non-ambulatory type 3 spinal muscular atrophy: a randomised, double-blind, placebo-controlled phase 2 trial. *Lancet Neurol* 16: 513–522, 2017. doi:10.1016/S1474-4422(17)30085-6.

10. Roche. (2018/05/18). Roche Releases Community Statement on Olesoxime Program (Online). Cure SMA, 2018. https://www.curesma.org/roche-releases-community-statement-on-olesoxime-program/.

11. **Muntoni F, Bertini E, Comi G, Kirschner J, Lusakowska A, Mercuri E, Scoto M, van der Pol WL, Vuillerot C, Burdeska A, El-Khairi M, Fontoura P, Ives J, Gorni K, Reid C, Fuerst-Recktenwald S; OLEOS Study Group.** Long-term follow-up of patients with type 2 and non-ambulant type 3 spinal muscular atrophy (SMA) treated with olesoxime in the OLEOS trial. *Neuromuscul Disord* 30: 959–969, 2020. doi:10.1016/j.nmd.2020.10.008.

12. **Ascah A, Khairallah M, Daussin F, Bourcier-Lucas C, Godin R, Allen BG, Petrof BJ, Rosiers CD, Burelle Y.** Stress-induced opening of the permeability transition pore in the dystrophin-deficient heart is attenuated by acute treatment with sildenafil. *Am J Physiol Heart Circ Physiol* 300: H144–H153, 2011. doi:10.1152/ajpheart.00522.2010.

13. **Godin R, Daussin F, Matecki S, Li T, Petrof BJ, Burelle Y.** Peroxisome proliferator-activated receptor γ coactivator 1-α gene transfer restores mitochondrial biomass and improves mitochondrial calcium handling in post-necrotic mdx mouse skeletal muscle. *J Physiol* 590: 5487–5502, 2012. doi:10.1113/jphysiol.2012.240390.

14. **Hughes MC, Ramos SV, Turnbull PC, Rebalka IA, Cao A, Monaco CMF, Varah NE, Edgett BA, Huber JS, Tadi P, Delfinis LJ, Schlattner U, Simpson JA, Hawke TJ, Perry CGR.** Early myopathy in Duchenne muscular dystrophy is associated with elevated mitochondrial H_2O_2 emission during impaired oxidative phosphorylation. *J Cachexia Sarcopenia Muscle* 10: 643–661, 2019. doi:10.1002/jcsm.12405.

15. **Abitbol J, Verschueren A, LaComblez L, Cuvier V, Jouve E, Pruss R, Blin O, Meininger V, Pouget J.** TRO19622 is well tolerated and achieves target plasma concentrations in a Phase Ib study in ALS patients. *Soc Neurosci Ann Meet*, 2007.

16. **Ramos SV, Hughes MC, Delfinis LJ, Bellissimo CA, Perry CGR.** Mitochondrial bioenergetic dysfunction in the D2.mdx model of

17. Duchenne muscular dystrophy is associated with microtubule disorganization in skeletal muscle. *PLoS One* 15: e0237138, 2020. doi:10.1371/journal.pone.0237138.

18. **Hughes MC, Ramos SV, Turnbull PC, Edgett BA, Huber JS, Polidovitch N, Schlattner U, Backx PH, Simpson JA, Perry CGR.** Impairments in left ventricular mitochondrial bioenergetics precede overt cardiac dysfunction and remodelling in Duchenne muscular dystrophy. *J Physiol* 598: 1377–1392, 2020. doi:10.1113/JP277306.

19. **Holmes DJ.** DBA/2 mouse. *Sci Aging Knowl Environ* 2003: as3, 2003. doi:10.1126/sageke.2003.44.as3.

20. **Xiao WH, Zheng FY, Bennett GJ, Bordet T, Pruss RM.** Olesoxime (cholest-4-en-3-one, oxime): analgesic and neuroprotective effects in a rat model of painful peripheral neuropathy produced by the chemotherapeutic agent, paclitaxel. *Pain* 147: 202–209, 2009. doi:10.1016/j.pain.2009.09.006.

21. **Martin LJ.** Olesoxime, a cholesterol-like neuroprotectant for the potential treatment of amyotrophic lateral sclerosis. *IDrugs* 13: 568–580, 2010.

22. **Butchbach ME, Edwards JD, Schussler KR, Burghes AH.** A novel method for oral delivery of drug compounds to the neonatal SMNΔ7 mouse model of spinal muscular atrophy. *J Neurosci Methods* 161: 285–290, 2007. doi:10.1016/j.jneumeth.2006.11.002.

23. **Gibbs EM, Crosbie-Watson RH.** A simple and low-cost assay for measuring ambulation in mouse models of muscular dystrophy. *JoVE* 130: e56772 2017. doi:10.3791/56772.

24. **Fajardo VA, Smith IC, Bombardier E, Chambers PJ, Quadrilatero J, Tupling AR.** Diaphragm assessment in mice overexpressing phospholamban in slow-twitch type I muscle fibers. *Brain Behav* 6: e00470, 2016. doi:10.1002/brb3.470.

25. **Gregorevic P, Plant DR, Lynch GS.** Administration of insulin-like growth factor-I improves fatigue resistance of skeletal muscles from dystrophic mdx mice. *Muscle Nerve* 30: 295–304, 2004. doi:10.1002/mus.20082.

26. **Moorwood C, Liu M, Tian Z, Barton ER.** Isometric and eccentric force generation assessment of skeletal muscles isolated from murine models of muscular dystrophies. *JoVE* 17: e50036, 2013. doi:10.3791/50036-v.

27. **Méndez J, Keys AB.** Density and composition of mammalian muscle. *Metab Clin Exp* 9: 184–188, 1960.

28. **Perry CG, Kane DA, Lin CT, Kozy R, Cathey BL, Lark DS, Kane CL, Brophy PM, Gavin TP, Anderson EJ, Neufer PD.** Inhibiting myosin-ATPase reveals a dynamic range of mitochondrial respiratory control in skeletal muscle. *Biochem J* 437: 215–222, 2011. doi:10.1042/BJ20110366.

29. **Fisher-Wellman KH, Gilliam LAA, Lin CT, Cathey BL, Lark DS, Darrell Neufer P.** Mitochondrial glutathione depletion reveals a novel role for the pyruvate dehydrogenase complex as a key H_2O_2-emitting source under conditions of nutrient overload. *Free Radic Biol Med* 65: 1201–1208, 2013. doi:10.1016/j.freeradbiomed.2013.09.008.

30. **Walsh B, Tonkonogi M, Söderlund K, Hultman E, Saks V, Sahlin K.** The role of phosphorylcreatine and creatine in the regulation of mitochondrial respiration in human skeletal muscle. *J Physiol* 537: 971–978, 2001. doi:10.1111/j.1469-7793.2001.00971.x.

31. **Perry CG, Kane DA, Lanza IR, Neufer PD.** Methods for assessing mitochondrial function in diabetes. *Diabetes* 62: 1041–1053, 2013. doi:10.2337/db12-1219.

32. **Ydfors M, Hughes MC, Laham R, Schlattner U, Norrbom J, Perry CG.** Modelling in vivo creatine/phosphocreatine in vitro reveals divergent adaptations in human muscle mitochondrial respiratory control by ADP after acute and chronic exercise. *J Physiol* 594: 3127–3140, 2016. doi:10.1113/JP271259.

33. **Fisher-Wellman KH, Mattox TA, Thayne K, Katunga LA, La Favor JD, Neufer PD, Hickner RC, Wingard CJ, Anderson EJ.** Novel role for thioredoxin reductase-2 in mitochondrial redox adaptations to obesogenic diet and exercise in heart and skeletal muscle. *J Physiol* 591: 3471–3486, 2013. doi:10.1113/jphysiol.2013.254193.

34. **Tsien RY.** Fluorescent Probes of Cell Signaling. *Annu Rev Neurosci* 12: 227–253, 1989. doi:10.1146/annurev.ne.12.030189.001303.

35. **Bloemberg D, Quadrilatero J.** Rapid determination of myosin heavy chain expression in rat, mouse, and human skeletal muscle using multicolor immunofluorescence analysis. *PLoS One* 7: e35273, 2012. doi:10.1371/journal.pone.0035273.

36. **Dam AD**, **Mitchell AS**, **Rush JW**, **Quadrilatero J.** Elevated skeletal muscle apoptotic signaling following glutathione depletion. *Apoptosis* 17: 48–60, 2012. doi:10.1007/s10495-011-0654-5.

37. **McMillan EM**, **Quadrilatero J.** Differential apoptosis-related protein expression, mitochondrial properties, proteolytic enzyme activity, and DNA fragmentation between skeletal muscles. *Am J Physiol Regul Integr Comp Physiol* 300: R531–R543, 2011. doi:10.1152/ajpregu.00488.2010.

38. **Mandel ER**, **Dunford EC**, **Abdifarkosh G**, **Turnbull PC**, **Perry CGR**, **Riddell MC**, **Haas TL.** The superoxide dismutase mimetic tempol does not alleviate glucocorticoid-mediated rarefaction of rat skeletal muscle capillaries. *Physiol Rep* 5: e13243, 2017. doi:10.14814/phy2.13243.

39. **Schlattner U**, **Möckli N**, **Speer O**, **Werner S**, **Wallimann T.** Creatine kinase and creatine transporter in normal, wounded, and diseased skin. *J Invest Dermatol* 118: 416–423, 2002. doi:10.1046/j.0022-202x.2001.01697.x.

40. **Sloan RC**, **Moukdar F**, **Frasier CR**, **Patel HD**, **Bostian PA**, **Lust RM**, **Brown DA.** Mitochondrial permeability transition in the diabetic heart: contributions of thiol redox state and mitochondrial calcium to augmented reperfusion injury. *J Mol Cell Cardiol* 52: 1009–1018, 2012. doi:10.1016/j.yjmcc.2012.02.009.

41. **Frasier CR**, **Moukdar F**, **Patel HD**, **Sloan RC**, **Stewart LM**, **Alleman RJ**, **La Favor JD**, **Brown DA.** Redox-dependent increases in glutathione reductase and exercise preconditioning: role of NADPH oxidase and mitochondria. *Cardiovasc Res* 98: 47–55, 2013. doi:10.1093/cvr/cvt009.

42. **Noble A**, **Guille M**, **Cobley JN.** ALISA: A microplate assay to measure protein thiol redox state. *Free Radic Biol Med* 174: 272–280, 2021. doi:10.1016/j.freeradbiomed.2021.08.018.

43. **Howell D.** *Fundamental Statistics for Behavioral Sciences*. Belmont, California: Wadsworth Cengage Learning 2011, p. 677.

44. **Meier U.** A note on the power of Fisher's least significant difference procedure. *Pharm Stat* 5: 253–263, 2006. doi:10.1002/pst.210.

45. **Aliev M**, **Guzun R**, **Karu-Varikmaa M**, **Kaambre T**, **Wallimann T**, **Saks V.** Molecular system bioenergics of the heart: experimental studies of metabolic compartmentation and energy fluxes versus computer modeling. *Int J Mol Sci* 12: 9296–9331, 2011. doi:10.3390/ijms12129296.

46. **Guzun R**, **Gonzalez-Granillo M**, **Karu-Varikmaa M**, **Grichine A**, **Usson Y**, **Kaambre T**, **Guerrero-Roesch K**, **Kuznetsov A**, **Schlattner U**, **Saks V.** Regulation of respiration in muscle cells in vivo by VDAC through interaction with the cytoskeleton and MtCK within mitochondrial interactosome. *Biochim Biophys Acta* 1818: 1545–1554, 2012. doi:10.1016/j.bbamem.2011.12.034.

47. **Wallimann T**, **Tokarska-Schlattner M**, **Schlattner U.** The creatine kinase system and pleiotropic effects of creatine. *Amino Acids* 40: 1271–1296, 2011. doi:10.1007/s00726-011-0877-3.

48. **Meyer RA**, **Sweeney HL**, **Kushmerick MJ.** A simple analysis of the "phosphocreatine shuttle". *Am J Physiol Cell Physiol* 246: C365–C377, 1984. doi:10.1152/ajpcell.1984.246.5.C365.

49. **Schlattner U**, **Kay L**, **Tokarska-Schlattner M.** Mitochondrial proteolipid complexes of creatine kinase. *Subcell Biochem* 87: 365–408, 2018. doi:10.1007/978-981-10-7757-9_13.

50. **Bessman SP**, **Fonyo A.** The possible role of the mitochondrial bound creatine kinase in regulation of mitochondrial respiration. *Biochem Biophys Res Commun* 22: 597–602, 1966. doi:10.1016/0006-291x(66)90317-2.

51. **Meyer LE**, **Machado LB**, **Santiago AP**, **da-Silva WS**, **De Felice FG**, **Holub O**, **Oliveira MF**, **Galina A.** Mitochondrial creatine kinase activity prevents reactive oxygen species generation: antioxidant role of mitochondrial kinase-dependent ADP re-cycling activity. *J Biol Chem* 281: 37361–37371, 2006. doi:10.1074/jbc.M604123200.

52. **Perry CG**, **Heigenhauser GJ**, **Bonen A**, **Spriet LL.** High-intensity aerobic interval training increases fat and carbohydrate metabolic capacities in human skeletal muscle. *Appl Physiol Nutr Metab* 33: 1112–1123, 2008. doi:10.1139/H08-097.

53. **Schlattner U**, **Tokarska-Schlattner M**, **Wallimann T.** Mitochondrial creatine kinase in human health and disease. *Biochim Biophys Acta* 1762: 164–180, 2006. doi:10.1016/j.bbadis.2005.09.004.

54. **Schlattner U**, **Tokarska-Schlattner M**, **Ramirez S**, **Brückner A**, **Kay L**, **Polge C**, **Epand RF**, **Lee RM**, **Lacombe M-L**, **Epand RM.** Mitochondrial kinases and their molecular interaction with cardiolipin. *Biochim Biophys Acta* 1788: 2032–2047, 2009. doi:10.1016/j.bbamem.2009.04.018.

55. **Datler C**, **Pazarentzos E**, **Mahul-Mellier AL**, **Chaisaklert W**, **Hwang MS**, **Osborne F**, **Grimm S.** CKMT1 regulates the mitochondrial permeability transition pore in a process that provides evidence for alternative forms of the complex. *J Cell Sci* 127: 1816–1828, 2014. doi:10.1242/jcs.140467.

56. **Bernardi P**, **Carraro M**, **Lippe G.** The mitochondrial permeability transition: recent progress and open questions. *FEBS J* 289: 7051–7074, 2021. doi:10.1111/febs.16254.

57. **Tantral L**, **Malathi K**, **Kohyama S**, **Silane M**, **Berenstein A**, **Jayaraman T.** Intracellular calcium release is required for caspase-3 and -9 activation. *Cell Biochem Funct* 22: 35–40, 2004. doi:10.1002/cbf.1050.

58. **Petronilli V**, **Penzo D**, **Scorrano L**, **Bernardi P**, **Di Lisa F.** The mitochondrial permeability transition, release of cytochrome c and cell death. Correlation with the duration of pore openings in situ. *J Biol Chem* 276: 12030–12034, 2001. doi:10.1074/jbc.M010604200.

59. **Budihardjo I**, **Oliver H**, **Lutter M**, **Luo X**, **Wang X.** Biochemical pathways of caspase activation during apoptosis. *Annu Rev Cell Dev Biol* 15: 269–290, 1999. doi:10.1146/annurev.cellbio.15.1.269.

60. **Bock FJ**, **Tait SWG.** Mitochondria as multifaceted regulators of cell death. *Nat Rev Mol Cell Biol* 21: 85–100, 2020. doi:10.1038/s41580-019-0173-8.

61. **Moore TM**, **Lin AJ**, **Strumwasser AR**, **Cory K**, **Whitney K**, **Ho T**, **Ho T**, **Lee JL**, **Rucker DH**, **Nguyen CQ**, **Yackly A**, **Mahata SK**, **Wanagat J**, **Stiles L**, **Turcotte LP**, **Crosbie RH**, **Zhou Z.** Mitochondrial dysfunction is an early consequence of partial or complete dystrophin loss in mdx mice. *Front Physiol* 11: 690, 2020. doi:10.3389/fphys.2020.00690.

62. **Ventura-Clapier R**, **Kuznetsov A**, **Veksler V**, **Boehm E**, **Anflous K.** Functional coupling of creatine kinases in muscles: species and tissue specificity. *Mol Cell Biochem* 184: 231–247, 1998.

63. **Perry CG**, **Kane DA**, **Herbst EA**, **Mukai K**, **Lark DS**, **Wright DC**, **Heigenhauser GJ**, **Neufer PD**, **Spriet LL**, **Holloway GP.** Mitochondrial creatine kinase activity and phosphate shuttling are acutely regulated by exercise in human skeletal muscle. *J Physiol* 590: 5475–5486, 2012. doi:10.1113/jphysiol.2012.234682.

64. **Ventura-Clapier R**, **Vassort G.** Role of myofibrillar creatine kinase in the relaxation of rigor tension in skinned cardiac muscle. *Pflugers Arch* 404: 157–161, 1985. doi:10.1007/BF00585412.

65. **Kuznetsov AV**, **Tiivel T**, **Sikk P**, **Kaambre T**, **Kay L**, **Daneshrad Z**, **Rossi A**, **Kadaja L**, **Peet N**, **Seppet E**, **Saks VA.** Striking differences between the kinetics of regulation of respiration by ADP in slow-twitch and fast-twitch muscles in vivo. *Eur J Biochem* 241: 909–915, 1996. doi:10.1111/j.1432-1033.1996.00909.x.

66. **Jones DP.** Radical-free biology of oxidative stress. *Am J Physiol Cell Physiol* 295: C849–C868, 2008. doi:10.1152/ajpcell.00283.2008.

67. **Sies H.** Oxidative stress: a concept in redox biology and medicine. *Redox Biol* 4: 180–183, 2015. doi:10.1016/j.redox.2015.01.002.

68. **Nicholls DG**, **Ferguson SJ.** *Bioenergetics 4*. The Netherlands: Elsevier, 2013.

69. **Weber JJ**, **Clemensson LE**, **Schiöth HB**, **Nguyen HP.** Olesoxime in neurodegenerative diseases: scrutinising a promising drug candidate. *Biochem Pharmacol* 168: 305–318, 2019. doi:10.1016/j.bcp.2019.07.002.

70. **Pozzan T**, **Bragadin M**, **Azzone GF.** Disequilibrium between steady-state Ca2+ accumulation ratio and membrane potential in mitochondria. Pathway and role of Ca2+ efflux. *Biochemistry* 16: 5618–5625, 1977. doi:10.1021/bi00644a036.

71. **Wrogemann K**, **Pena SDJ.** Mitochondrial calcium overload: a general mechanism for cell-necrosis in muscle diseases. *Lancet* 307: 672–674, 1976. doi:10.1016/s0140-6736(76)92781-1.

72. **Robert V**, **Massimino ML**, **Tosello V**, **Marsault R**, **Cantini M**, **Sorrentino V**, **Pozzan T.** Alteration in calcium handling at the subcellular level in mdx myotubes. *J Biol Chem* 276: 4647–4651, 2001. doi:10.1074/jbc.M006337200.

73. **Leijendekker WJ**, **Passaquin AC**, **Metzinger L**, **Rüegg UT.** Regulation of cytosolic calcium in skeletal muscle cells of the mdx mouse under conditions of stress. *Br J Pharmacol* 118: 611–616, 1996. doi:10.1111/j.1476-5381.1996.tb15445.x.

74. **Eckmann J**, **Clemens LE**, **Eckert SH**, **Hagl S**, **Yu-Taeger L**, **Bordet T**, **Pruss RM**, **Muller WE**, **Leuner K**, **Nguyen HP**, **Eckert GP.** Mitochondrial membrane fluidity is consistently increased in different

models of Huntington disease: restorative effects of olesoxime. *Mol Neurobiol* 50: 107–118, 2014. doi:10.1007/s12035-014-8663-3.

75. **Weber JJ**, **Ortiz Rios MM**, **Riess O**, **Clemens LE**, **Nguyen HP.** The calpain-suppressing effects of olesoxime in Huntington's disease. *Rare Dis* 4: e1153778, 2016 [Erratum in doi: 10.1093/brain/awv290]. doi:10.1080/21675511.2016.1153778.

76. **Ciafaloni E**, **Kumar A**, **Liu K**, **Pandya S**, **Westfield C**, **Fox DJ**, **Caspers Conway KM**, **Cunniff C**, **Mathews K**, **West N**, **Romitti PA**, **McDermott MP.** Age at onset of first signs or symptoms predicts age at loss of ambulation in Duchenne and Becker muscular dystrophy: data from the MD STARnet. *J Pediatr Rehabil Med* 9: 5–11, 2016. doi:10.3233/PRM-160361.

77. **Dubinin MV**, **Talanov EY**, **Tenkov KS**, **Starinets VS**, **Mikheeva IB**, **Sharapov MG**, **Belosludtsev KN.** Duchenne muscular dystrophy is associated with the inhibition of calcium uniport in mitochondria and an increased sensitivity of the organelles to the calcium-induced permeability transition. *Biochim Biophys Acta Mol Basis Dis* 1866: 165674, 2020. doi:10.1016/j.bbadis.2020.165674.

78. **Buyse GM**, **Goemans N**, **van den Hauwe M**, **Thijs D**, **de Groot IJ**, **Schara U**, **Ceulemans B**, **Meier T**, **Mertens L.** Idebenone as a novel, therapeutic approach for Duchenne muscular dystrophy: results from a 12 month, double-blind, randomized placebo-controlled trial. *Neuromuscul Disord* 21: 396–405, 2011. doi:10.1016/j.nmd.2011.02.016.

79. **Buyse GM**, **Voit T**, **Schara U**, **Straathof CSM**, **D'Angelo MG**, **Bernert G**, **Cuisset J-M**, **Finkel RS**, **Goemans N**, **McDonald CM**, **Rummey C**, **Meier T**; **DELOS Study Group.** Efficacy of idebenone on respiratory function in patients with Duchenne muscular dystrophy not using glucocorticoids (DELOS): a double-blind randomised placebo-controlled phase 3 trial. *Lancet* 385: 1748–1757, 2015. doi:10.1016/S0140-6736(15)60025-3.